zürich 2024

FDD

European Hyperloop Week

Tachyon Hyperloop

March 17, 2024

EUROPEAN HYPERLOOP WEEK

Contents

Introduction

Tachyon Hyperloop e.V. is a pioneering initiative conceived in 2019 by students from RWTH Aachen University and FH Aachen University of Applied Sciences. Inspired by Elon Musk's groundbreaking vision of the Hyperloop in 2013, our team comprises 35 dedicated students from diverse academic backgrounds, all unified by our shared commitment to pushing the boundaries of knowledge and technology within the transportation sector.

Our team functions seamlessly across six specialized departments: Mechanical, Electrical, Project Management, Business and Marketing, Sponsoring, and Architecture & Urban Design. Each department is led by a proficient team lead, ensuring clear communication and effective coordination across all project facets. Guided by the strategic oversight of board members including Jacob Diercks, Marijan Schlösser, and Yashasvi Karnena, we navigate the complex landscape of Hyperloop innovation with determination and vision.

1.1 FDD.7 Applicant and List of Team Members

1.2 FDD.8 Development Environment and Research Objectives

Despite the demands of our academic pursuits, we dedicate ourselves fully to the Tachyon initiative. From our inception, we have found a home at the Collective Incubator, a vibrant hub that fosters collaboration and innovation. Previously, we benefited from the facilities at the WZL, an institute of RWTH Aachen University, before transitioning to our current workspace. This dynamic environment has nurtured our growth and facilitated the realization of our ambitious projects.

Our endeavors are sustained through a blend of financial support from sponsors, generous donations, and contributions from supporting organizations. Tachyon Hyperloop epitomizes our collective aspiration to design and construct functional prototypes of Hyperloop Pods, contributing significantly to the advancement of transportation technology on a global scale.

Acknowledging our sponsors is pivotal to the success of our projects. We extend our heartfelt appreciation to RWTH Aachen University for their unwavering support throughout our journey. Special gratitude is also extended to Institut für Allgemeine Mechanik for their invaluable expertise and infrastructure. Additionally, we express our gratitude to proRWTH, WZL, and International Academy for their unwavering support. We extend our heartfelt thanks to EVS Euregio GmbH for providing a testing track and to Collective Incubator e.V. for their provision of an exceptional office space. Special thanks are extended to our sponsor-partners STAWAG, Emrax, Mouser, Contitech AG, Leaddrive, Vector, PWC and Dürr for their substantial material and financial support. Finally, we would like to express our appreciation to the European Hyperloop Week Committee for providing us with the opportunity to showcase our project, facilitating collaboration, information sharing, and networking within the Hyperloop community.

Apart from our primary projects highlighted in this documentation, Tachyon Hyperloop e.V. is also engaged in other initiatives that are integral to our research and development.

One such project is Pathfinder. As one of the few teams to have our own test track near Aachen, generously provided by our partner EVS EUREGIO Verkehrsschienennetz GmbH, our 1 km long test

track stands as one of the longest among student teams. For the upcoming European Hyperloop Week 2024 competition, we have collaborated with Swissloop to utilize their track infrastructure. This partnership aims to foster knowledge exchange, allowing us to gain valuable insights into the limitations and advantages of their track design. By sharing the same tracks, we also anticipate significant cost efficiencies. The strategic collaboration between our teams promises mutual benefits, facilitating innovation and advancement within the Hyperloop community.

Additionally, the Minipod project plays a vital role in our development process. Serving as a prototype of the prototype, the Minipod enables us to mitigate risks associated with resource allocation and system functionality before implementing them on a larger scale. By developing and testing on a smaller scale, we can gather valuable insights and refine our technologies with reduced risk.

In the upcoming sections, we will delve into a comprehensive System Overview, offering a succinct understanding of the Pod. Following this, we will explore the Mechanical system, intricately detailing the design and construction of our pod. Our focus will then shift to the Electrical domain, where we will discuss vital components such as the Sense & Control systems crucial for our pod's functionality. Additionally, we will address Safety measures implemented to ensure the well-being of our team and the success of of our project. Through these sections, our aim is to provide a detailed insight into our project's development process, while adhering to the guidelines and regulations outlined by the European Hyperloop Week Committee.

1.3 FDD.10 Category for This Application

Name	Department
Jacob Dierck	First Chairman
Marijan Schlösser	Second Chairman
Yashasvi Karnena	Treasurer
Pascal Pfeifer	Mechanical Department
Lennart Jepsen	Mechanical Department
Niclas Vermeulen	Mechanical Department
Shreepad Khedkar	Mechanical Department
Benjamin Köhler	Mechanical Department
Jasmin Dedeoglu	Mechanical Department
Aniket Saxena	Mechanical Department
Kanishk Singh	Mechanical Department
Yash Shah	Mechanical Department
Rengin Solmaz	Mechanical Department
Sachin Salaskar	Mechanical Department
Guru Bysani	Mechanical Department
Aryan Modi	Mechanical Department
Vaishnavi Ramkumar	Mechanical Department
Dino Cheng	Electrical Department
Abhishek Jha	Electrical Department
Sourajit Majumder	Electrical Department
Stefan Boskovic	Electrical Department
Bohdan Popov	Electrical Department
Ian Morales	Electrical Department
Paula Vicente	Electrical Department
Aryan Kumalajati	Electrical Department
Praneet Tuli	Project Management
Duc Thiem Do	Project Management
Till Behringer	Project Management
Ludwig Gatzsch	Business & Marketing
Henriette Brucks	Business & Marketing
Joana Baumann	Sponsoring
Carl-Philipp Schetelig	Sponsoring
Clara Kamrath	Architecture & Urban Design
Hannes Wittkopf	Architecture & Urban Design
Janik Hiob	Architecture & Urban Design

Table 1.1: Team Members and Departments

Mechanical Systems

2.1 Introduction

2.2 Chassis

2.2.1 Overview

Requirements and Constraints

Paramount among our requirements is the ability of the chassis to withstand the rigors of operation, with a primary focus on supporting a load of up to 250 kg. The chassis must serve as the sturdy foundation upon which all subsystems are mounted. From the propulsion system to the suspension components, every subsystem must find its place within the chassis.

A chassis that is inaccessible is as good as useless. Hence, a key requirement driving our design is the ease of access for maintenance and assembly. Components must be readily accessible, allowing for swift troubleshooting and efficient assembly processes. The chassis must seamlessly integrate with the aeroshell, providing a secure mounting point while ensuring aerodynamic efficiency. This requirement necessitates careful consideration of mounting points and structural reinforcements to support the aeroshell without compromising performance.

Weight is the enemy of performance, and our chassis must strike a delicate balance between structural robustness and lightweight construction. Utilizing advanced materials and optimization techniques, we aim to minimize weight without compromising strength or durability.

While performance is paramount, cost considerations cannot be overlooked. Our chassis must be constructed in a manner that balances performance with affordability, ensuring that our project remains economically viable without sacrificing quality or functionality. The chassis must withstand the dynamic forces exerted by both the braking system and the suspension components.

This constraint necessitates careful reinforcement and structural design to ensure that the chassis remains resilient under varying load conditions. The design must incorporate provisions for easy extraction of the battery pack, facilitated by a rail system. This constraint imposes additional design considerations, such as clearance and mounting points, to ensure seamless integration and accessibility.

Concept

The chassis plays an important role in any moving structure, providing the structural foundation and support necessary to ensure safety, stability, and functionality for the entire vehicle and all the systems it holds. In this year's iteration, our pod utilises a two-track system, which not only allows for extra room to house subsystems but also lowers the pod's centre of mass, thereby enhancing stability. This design decision results in a wider and consequently shorter pod.

At the core of our design philosophy lies the integration of carbon fiber sandwich plates, a cutting-edge material renowned for its exceptional strength-to-weight ratio and structural integrity.

The foundation of our chassis is built upon a rectangular framework, strategically crafted to optimize both stability and versatility. Covering the entirety of the lower section of the pod is a ground plate, providing a robust foundation while simultaneously enhancing aerodynamic efficiency. This ground plate serves as the backbone of the chassis, ensuring unparalleled stability and structural integrity.

Extending longitudinally from the front to the back of the pod are two key components: the longitudinal plates. These plates constitute the primary structural elements of the chassis, serving as the anchor points for vital components such as the suspension system, brakes, and motor. Crafted with precision and reinforced for maximum resilience, these longitudinal plates epitomize the marriage of form and function, providing the framework upon which our pod's performance hinges.

To further fortify the structural integrity of our chassis and prevent any potential bending or detachment of the longitudinal plates, we have strategically incorporated three additional cross panels. These panels, positioned perpendicular to the longitudinal plates, serve as stabilizing agents, distributing forces evenly throughout the chassis and bolstering overall rigidity. these cross panels ensure that our pod remains steadfast and unwavering, even under the most demanding conditions.

Central to the assembly of our chassis is a plug-in system, integrated into the carbon fiber sandwich plates. Through precision-cut cutouts and advanced adhesive technologies, these plates seamlessly interlock and adhere, forming a cohesive and resilient structure. This plug-in system not only streamlines the assembly process but also enhances the overall integrity of the chassis, ensuring a robust and reliable foundation for our pod.

Size, Components, and Appearance

Component	Number	Mass [kg]	Size [mm]	Material	Manufacturing process	In-house/ outsourced
GP	x1	1	1480x882x20	CF Sandwich	Waterjetcut	Outsourced
CacP	x1	1	882x200x20	CF Sandwich	Waterjetcut	Outsourced
BacP	x2	0.1	882x200x20	CF Sandwich	Waterjetcut	Outsourced
BCalP	x2	0.2	883x200x20	CF Sandwich	Waterjetcut	Outsourced
AalP	x2	0.2	270x200x20	CF Sandwich	Waterjetcut	Outsourced
Seam Type A	x2	0.1	1480x882x1	CF Prepeg	Cut	Outsourced
Seam Type B	x7	0.1	882x200x1	CF Prepeg	Cut	Outsourced
Seam Type C	x2	0.1	882x200x1	CF Prepeg	Cut	Outsourced
Seam Type D	x2	0.1	883x200x1	CF Prepeg	Cut	Outsourced
Crossbar	x2	0.5	270x200x20	Aluminium	Waterjetcut	Outsourced

Table 2.1: Components and Manufacturing Details

2.2.2 Theoretical concepts

WILL BE ADDED SOON

2.2.3 Design Process and Appearance

CAD Models and Technical Drawings

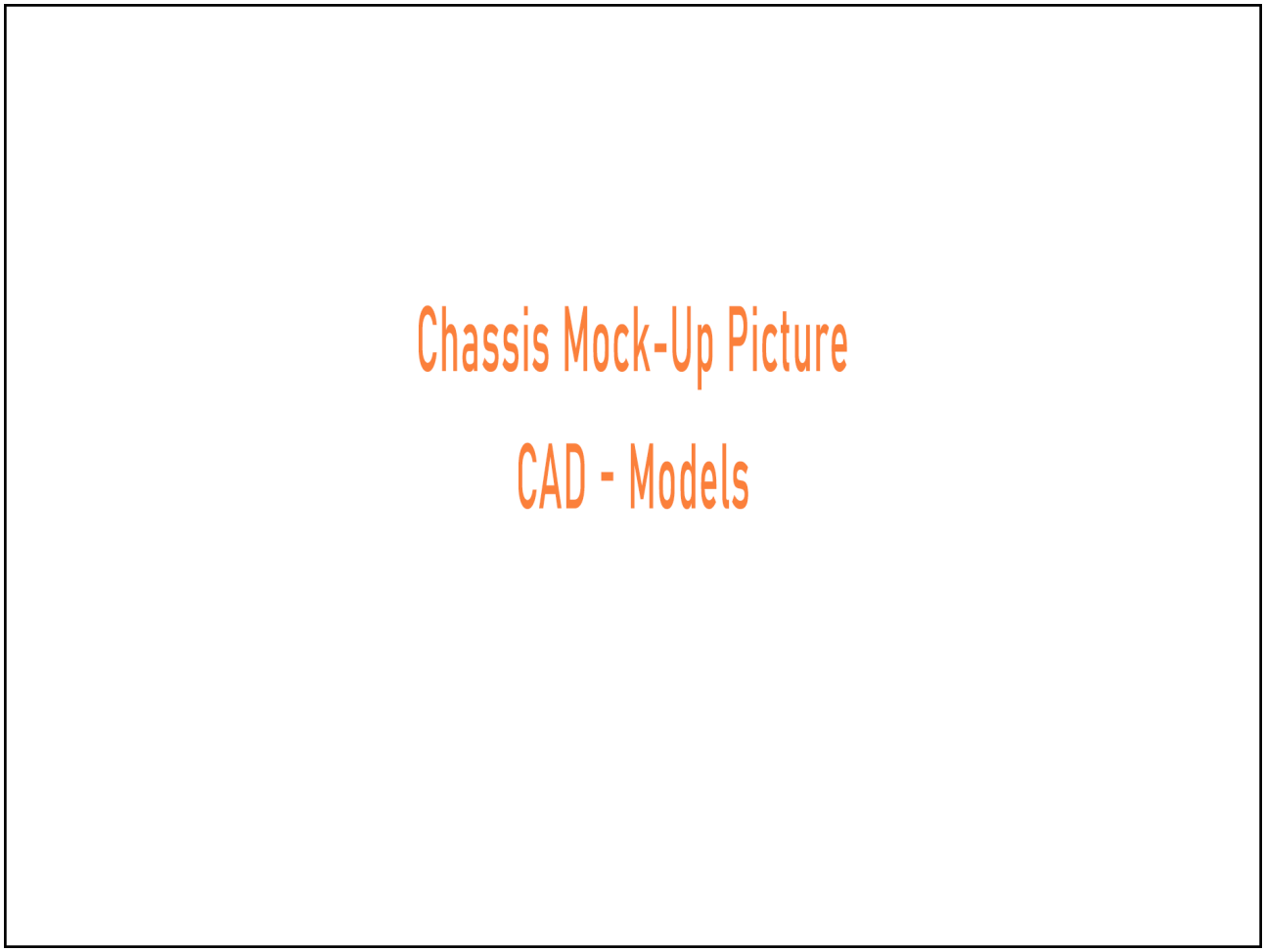

Figure 2.1: Caption for the image.

Materials

As discribed above the main factor for choosing carbon fiber sandwich panels was the the weight-strenght-cost balance. Choosing a foam-insert over a honeycomb-insert came down to the higher weather-resistants of the foam against cardboard. Again we chose carbonfiber over aluminum for the plates for lesser weight.

Design Rationale

The design rationale guiding our pod's infrastructure embodies a methodical process rooted in practical considerations and engineering principles. Our primary aim was to reduce weight from the previous design, leading us to explore the potential of carbon fiber composites.

Initially, a monocoque chassis was considered for its structural integrity, yet its high cost and manufacturing complexity deemed it impractical. Similarly, the idea of a tube chassis with carbon fiber tubes proved prohibitively expensive. Thus, we opted for a Composite Sandwich Panel Chassis, renowned for its lightweight, structural strength, and cost-effectiveness.

Departing from the original design, which featured longitudinal panels spanning the entire length of the pod, we recognized the necessity for easy battery extraction from the side, prompting a redesign of the chassis layout. To ensure seamless panel interlocking and structural integrity, we

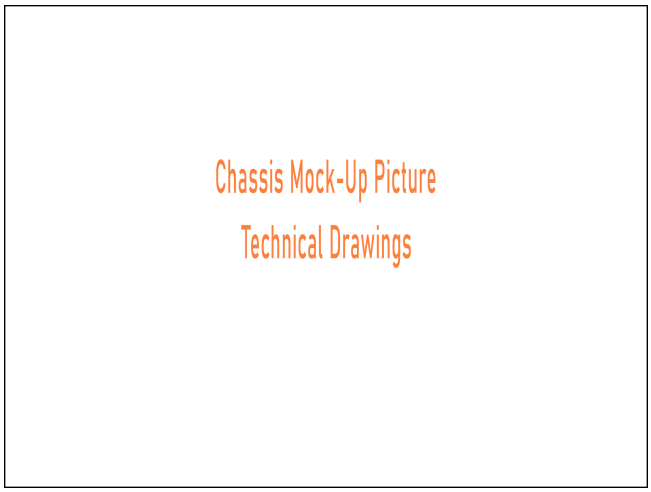

(a) Caption for the first image.

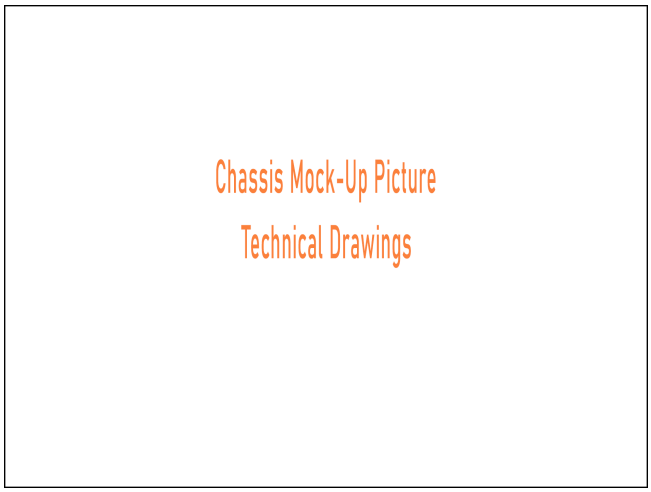

(b) Caption for the second image.

Figure 2.2: Caption for the whole figure.

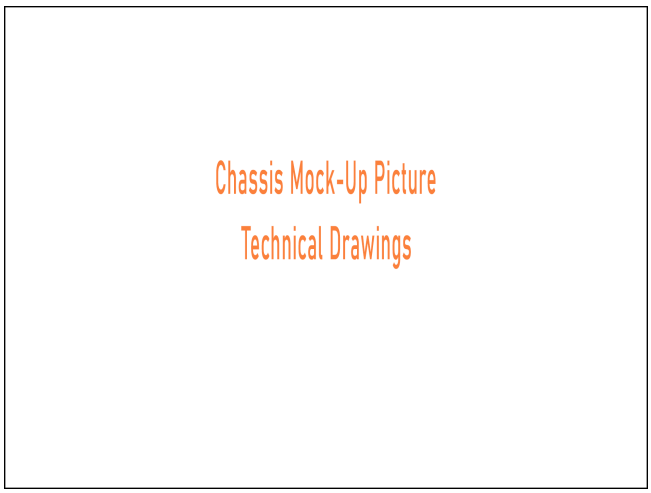

(a) Caption for the first image.

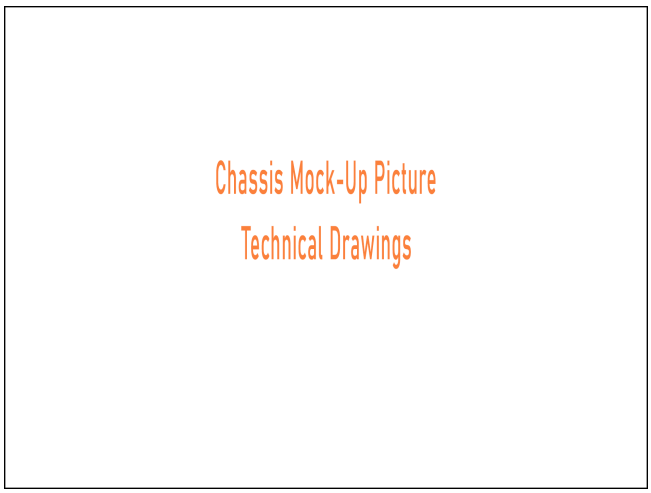

(b) Caption for the second image.

Figure 2.3: Caption for the whole figure.

devised a plug-in system featuring evenly distributed cutouts, meticulously aligned for connection. These connections are strengthened by precise gluing and reinforced seaming along the edges.

Additionally, crossbars were strategically integrated to fortify the chassis at suspension mounting points, mitigating potential structural weaknesses. Furthermore, close collaboration between the chassis department and other subsystems facilitated maximal compatibility and integration.

In summary, our design rationale represents a pragmatic synthesis of innovation and engineering expertise, driven by a commitment to efficiency, functionality, and cost-effectiveness.

FEM Results

Static Simulation Stress Test: In this simulation scenario, the chassis was subjected to a static stress test, replicating the forces exerted by the suspension system along with the weight of the pod. The FEM analysis yielded critical insights into the structural performance of the chassis under static loading conditions.

Results:

- Maximum von Mises stress: [Replace with your FEM result]
- Maximum principal stress: [Replace with your FEM result]

- Factor of safety: [Replace with your FEM result]

Interpretation: The FEM analysis indicates that under static loading conditions, the chassis exhibits [Replace with your interpretation of FEM results]. While localized areas may experience elevated stress levels, the overall factor of safety remains within acceptable limits, suggesting satisfactory structural integrity.

Braking Maneuver Simulation In this simulation scenario, the chassis underwent analysis with peak forces experienced during braking maneuvers, simulating the most demanding braking conditions. The FEM analysis provided crucial insights into the chassis's ability to withstand dynamic braking forces.

Results:

- Maximum von Mises stress: [Replace with your FEM result]
- Maximum principal stress: [Replace with your FEM result]
- Factor of safety: [Replace with your FEM result]

Interpretation: The FEM analysis reveals that during braking maneuvers, the chassis experiences [Replace with your interpretation of FEM results]. Despite localized stress concentrations, the overall factor of safety remains satisfactory, indicating adequate structural robustness.

Worst-Case Scenario: In the worst-case scenario simulation, the chassis was subjected to double the forces encountered in the previous scenarios, representing an extreme operating condition. This simulation aimed to assess the chassis's resilience under significantly elevated loading conditions.

Results:

- Maximum von Mises stress: [Replace with your FEM result]
- Maximum principal stress: [Replace with your FEM result]
- Factor of safety: [Replace with your FEM result]

Interpretation: The FEM analysis of the worst-case scenario indicates [Replace with your interpretation of FEM results]. Despite heightened stress levels, the factor of safety remains within acceptable limits, suggesting that the chassis can withstand double the expected forces without compromising structural integrity.

Conclusion: Overall, the FEM results provide valuable insights into the structural performance of the chassis under various loading conditions. These findings will inform further optimization efforts and ensure that the chassis meets stringent performance and reliability requirements.

Calculations

In order to ensure the accuracy and reliability of the Finite Element Method (FEM) simulations, it is crucial to provide a comprehensive justification for the simulated loads. The following reasoning and calculations support the chosen loads for each simulation scenario:

- Static Simulation Stress Test

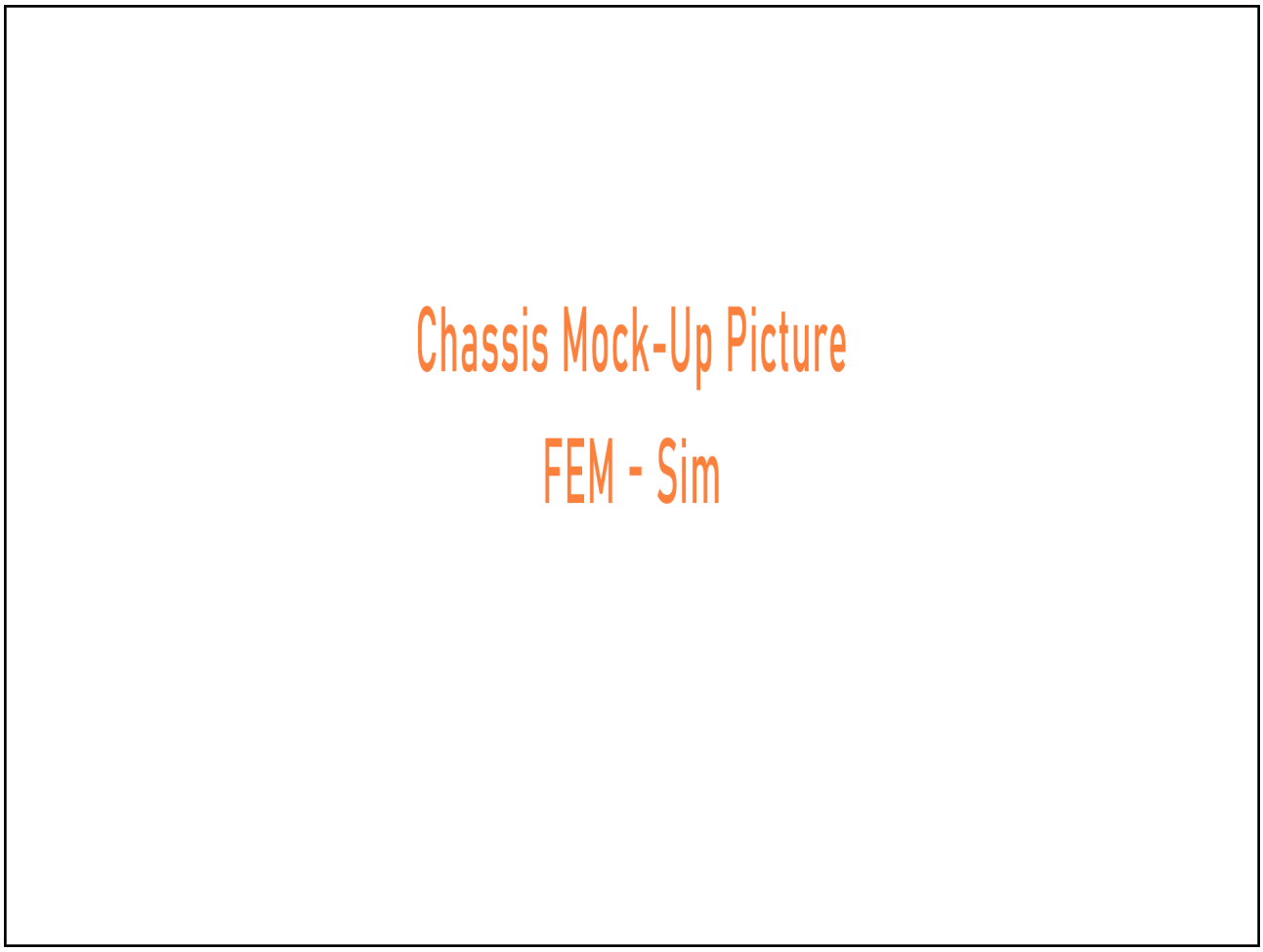

Figure 2.4: Caption for the image.

  - Reasoning: The static simulation stress test replicates the forces exerted by the suspension system and the weight of the pod when the vehicle is at rest or moving at a constant velocity. This scenario is essential to evaluate the chassis's ability to withstand static loading conditions, providing insights into its structural integrity and load-bearing capacity.
  - 1. Suspension Forces: The suspension system applies forces to the chassis, primarily in the vertical direction, to support the weight of the vehicle and absorb road irregularities.
  - Average Suspension Force (Fsus): (Insert calculation based on suspension design and vehicle weight distribution)
  - 2. Weight of the Pod: The weight of the pod contributes to the overall static loading on the chassis.
  - Pod Weight (Wpod): (Insert actual weight of the pod)
  - Total Load: Total Load = Suspension Forces + Weight of the Pod Total Load = Fsus + Wpod

- Braking Maneuver Simulation
  - Reasoning: The braking maneuver simulation replicates the peak forces experienced by the chassis during braking events. This scenario is crucial to assess the chassis's ability to withstand dynamic loading conditions, particularly during sudden deceleration, and ensure structural stability and safety.
  - 1. Peak Braking Force: The braking system applies forces to the chassis during braking maneuvers, primarily in the longitudinal direction, to decelerate the vehicle.

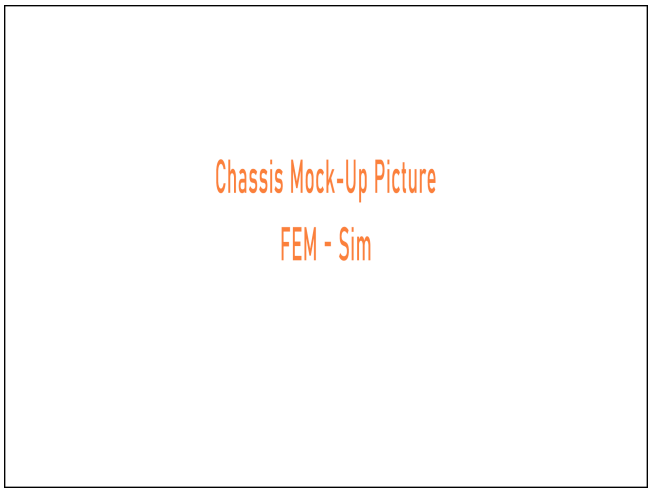

(a) Caption for the first image.

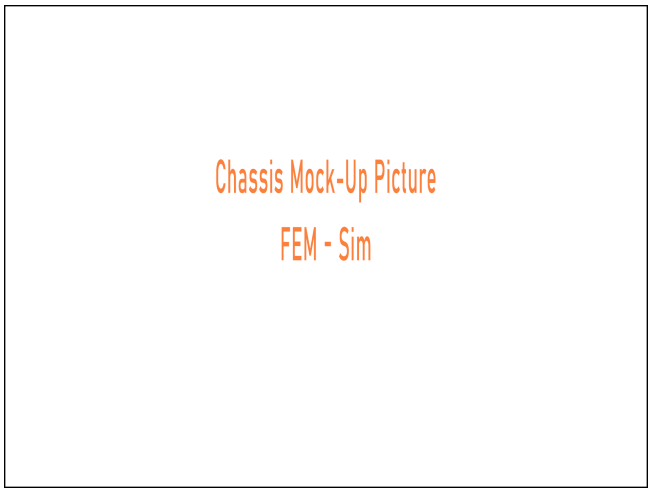

(b) Caption for the second image.

Figure 2.5: Caption for the whole figure.

- Peak Braking Force (Fbrake): (Insert calculation based on braking system specifications and vehicle weight)

- Worst-Case Scenario:
  - Reasoning: The worst-case scenario involves doubling the forces encountered in the previous scenarios, representing an extreme operating condition. This scenario tests the limits of the chassis's structural resilience and provides insights into its performance under significantly elevated loading conditions.
  - 1. Double Suspension Forces: The suspension forces are doubled to simulate extreme vertical loading conditions on the chassis. - Double Suspension Forces (2 □ Fsus)
  - 1. Double Braking Forces:The braking forces are doubled to simulate extreme braking maneuvers. - Double Braking Forces (2 □ Fbrake)
  - Conclusion: By providing rigorous justification and performing the necessary load calculations, we ensure that the simulated loads accurately represent real-world operating conditions. These simulations enable us to evaluate the structural performance of the chassis under various loading scenarios, guiding optimization efforts and ensuring the chassis meets stringent performance requirements.

- Acceleration due to gravity: $9.81 \frac{m}{s^2}$ - Weight of the pod (W_pod) = Mass of the pod × Acceleration due to gravity

2. Forces from Suspension: - Suspension force: [Replace with actual suspension force] - Total force from suspension (F_suspension) = Suspension force × Number of suspension points

3. Total Static Load: - Total static load = Weight of the pod + Total force from suspension

Simulation Scenario 2: Braking Maneuver Simulation

1. Peak Braking Force: - Maximum deceleration: [Replace with actual maximum deceleration] - Mass of the vehicle: [Replace with actual mass] - Peak braking force = Mass of the vehicle × Maximum deceleration

Worst-Case Scenario:

1. Double Forces: - Double weight of the pod: 2 × Weight of the pod - Double total

Mesh and Boundary Conditions

Mesh Type: For our Finite Element Method (FEM) simulations, we utilized a structured mesh approach, specifically employing a combination of hexahedral and tetrahedral elements. This mesh

type offers several advantages, including improved computational efficiency, better accuracy in capturing complex geometries, and reduced numerical error.

Boundary Conditions:

1. Fixed Constraints: - Suspension Mounting Points: The chassis is fixed at the suspension mounting points to simulate the rigid attachment of the suspension system to the chassis. - Ground Contact: The bottom surface of the chassis is fixed to simulate contact with the ground, ensuring realistic loading conditions.

2. Applied Loads: - Suspension Forces: Vertical forces are applied at the suspension mounting points to simulate the forces exerted by the suspension system on the chassis. These forces represent the weight of the vehicle and any additional loads imposed by the suspension system. - Braking Forces: Longitudinal forces are applied to simulate the braking forces exerted on the chassis during braking maneuvers. These forces are applied at the contact points between the braking system and the chassis.

3. Symmetry and Constraints: - Symmetry: Symmetry boundary conditions are applied to exploit the symmetry of the chassis geometry, reducing computational complexity and improving efficiency. - Constraints: Constraints are imposed on certain degrees of freedom to enforce realistic behavior and prevent unrealistic deformations or displacements.

4. Mesh Refinement: - Local Mesh Refinement: Mesh refinement techniques are applied in areas of geometric complexity or high stress concentration to ensure accurate representation of stress distribution and structural response.

Conclusion: By employing a structured mesh approach and carefully defining boundary conditions, we ensure that our FEM simulations accurately capture the behavior of the chassis under various loading scenarios. These simulations provide valuable insights into the structural performance of the chassis, guiding optimization efforts and ensuring that the design meets stringent performance requirements.

WILL BE ADDED SOON

2.2.4 Manufacturing Process

Firstly, the panels are sourced and procured in accordance with precise specifications, ensuring they meet the required size and shape criteria. Any necessary cutouts or holes are meticulously made in alignment with design specifications, utilizing advanced cutting techniques to ensure accuracy and consistency. Subsequently, support plates are precisely cut to the required size and shape, with corresponding holes carefully drilled to facilitate seamless integration with the panels.

These support plates serve a critical role in reinforcing the structural integrity of the chassis, providing additional strength and stability. Following preparation of the panels and support plates, a meticulous assembly process ensues. The support plates are methodically glued to the designated spots on the panels, adhering to precise positioning guidelines to ensure optimal alignment and functionality.

Once the support plates are securely affixed, the panels are carefully assembled and glued together, forming a cohesive structure that embodies the desired design configuration. This assembly process is executed with meticulous attention to detail, ensuring that each component is seamlessly integrated to achieve the desired structural integrity and functionality.

Finally, the seams between the assembled panels are meticulously cut to the required size and adhered to the edges of the plugged panels. This final step serves to further reinforce the structural integrity of the chassis while providing a polished finish that enhances both aesthetics and durability. Through adherence to this comprehensive manufacturing process, we ensure that the designed part is not only realized in a practical and efficient manner but also upholds the highest standards of quality and performance.

or:

Efforts have been undertaken to ensure that the designed part is realistically manufacturable, with a focus on simplicity, efficiency, and accessibility in manufacturing processes.

1. 2D Waterjet Cutting for Panels: Utilizing 2D waterjet cutting for the panels ensures precise and efficient fabrication. This method allows for accurate cutting of complex shapes and contours, facilitating the production of panels with minimal material wastage.

2. Scissor-Cut Seams: Seam cutting by scissors offers a straightforward and cost-effective approach to joining panels. This manual method provides flexibility and ease of assembly, allowing for adjustments as needed during the manufacturing process. Additionally, it eliminates the need for specialized equipment, reducing production costs and complexity.

3. Waterjet Cutting for Plates: Employing waterjet cutting for the plates ensures accurate and clean cuts, maintaining dimensional accuracy and quality. This method allows for the fabrication of support plates with intricate designs and precise hole placements, enabling optimal integration with the chassis components.

By leveraging these manufacturing techniques, we streamline the production process while maintaining the integrity and functionality of the designed part. The simplicity and accessibility of these methods ensure that the manufacturing process remains efficient, cost-effective, and scalable, ultimately contributing to the overall success of the project.

2.2.5 Integration process

Assembling

Firstly, the panels are sourced and procured in accordance with precise specifications, ensuring they meet the required size and shape criteria. Any necessary cutouts or holes are meticulously made in alignment with design specifications, utilizing advanced cutting techniques to ensure accuracy and consistency.

Subsequently, support plates are precisely cut to the required size and shape, with corresponding holes carefully drilled to facilitate seamless integration with the panels. These support plates serve a critical role in reinforcing the structural integrity of the chassis, providing additional strength and stability.

Following preparation of the panels and support plates, a meticulous assembly process ensues. The support plates are methodically glued to the designated spots on the panels, adhering to precise positioning guidelines to ensure optimal alignment and functionality.

Once the support plates are securely affixed, the panels are carefully assembled and glued together, forming a cohesive structure that embodies the desired design configuration. This assembly process is executed with meticulous attention to detail, ensuring that each component is seamlessly integrated to achieve the desired structural integrity and functionality.

Finally, the seams between the assembled panels are meticulously cut to the required size and adhered to the edges of the plugged panels. This final step serves to further reinforce the structural integrity of the chassis while providing a polished finish that enhances both aesthetics and durability.

Through adherence to this comprehensive manufacturing process, we ensure that the designed part is not only realized in a practical and efficient manner but also upholds the highest standards of quality and performance.

Assembly interaction

The interaction between subsystems within the pod is orchestrated with precision, each component playing a crucial role in ensuring seamless functionality and performance. At the heart of this interaction lies the chassis, serving as the sturdy backbone upon which all subsystems are mounted. The chassis not only provides structural support but also serves as a conduit for distributing forces generated by key subsystems such as the brakes, motor, and suspension.

The motor, positioned centrally within the pod, exerts significant forces that are channeled directly through the chassis. As the primary source of propulsion, the motor's torque and power

output directly influence the chassis's stability and performance. Similarly, the braking system, situated on the sides directly above the track, exerts substantial forces during deceleration. These forces are transmitted through the chassis, requiring robust structural reinforcement to withstand the resulting stresses.

The suspension system, located at the front and back ends of the pod, plays a critical role in ensuring ride comfort and handling. The forces generated by the suspension, particularly during cornering and uneven terrain traversal, are transmitted through the chassis, necessitating careful design considerations to maintain stability and responsiveness.

In addition to these dynamic subsystems, the electrical systems are integrated into the chassis using sheet metal and 3D-printed brackets. This strategic mounting ensures secure placement while minimizing interference with other components.

Furthermore, the battery, housed within a dedicated battery box, is mounted on telescopic rails affixed to the chassis. This arrangement not only facilitates easy access for maintenance but also ensures optimal weight distribution and stability.

Through integration and strategic mounting, each subsystem interacts harmoniously with the chassis and other components, collectively contributing to the overall functionality and performance of our pod. This cohesive interaction is essential for achieving our objectives of efficiency, reliability, and safety.

2.2.6 Safety Considerations

Safety Factor

For our project, we have established a minimum safety factor of n=2 for all structural elements. This means that the ultimate strength of each component must be at least twice the maximum expected load it will experience.

Reaching a safety factor of n=... provides a significant margin of safety, offering protection against unforeseen variations in loading conditions, material properties, and environmental factors. It ensures that the structural elements can withstand unexpected peak loads or transient events without compromising safety or integrity.

Worst-Case Scenarios

WILL BE ADDED SOON

2.2.7 FMEA Results Discussion

Risk Assessment

WILL BE ADDED SOON

FMEA and Risk Mitigation

Simulation Evidence

WILL BE ADDED SOON

2.2.8 Testing

Safety Procedures Documentation

The testing procedures for the hyperloop pod chassis are meticulously crafted to assess structural integrity, durability, and performance under conditions that closely simulate actual operation. The procedures outlined below provide a comprehensive approach to validating the chassis design.

Static Load Testing

- Objective: To evaluate the chassis's ability to withstand forces it would encounter while stationary.
- Procedure: Securely mount the chassis at suspension mounting holes. Apply a static load equivalent to twice the anticipated weight of the finished pod.
- Outcome: Determine load-bearing capacity and ensure no structural deformation or failure.

Dynamic Load Testing

- Objective: To assess the chassis's responsiveness and robustness under dynamic loading conditions.
- Procedure: Subject the chassis to simulated forces of acceleration, braking, and cornering. Collect data on how the chassis flexes and reacts under these conditions.
- Outcome: Confirm the chassis's integrity under dynamic stresses and identify potential areas for reinforcement.

Bending Stress Test

- Objective: To understand the material properties of the chassis, particularly its bending strength and ductility.
- Procedure: Fabricate a reference part from the same material as the chassis. Apply incremental force until the part fails, if applicable.
- Outcome: Ascertain the material's resistance to bending forces and its behavior under stress.

Vibration Testing

- Objective: To evaluate the chassis's ability to endure and dampen vibrations during operation.
- Procedure: Expose the chassis to controlled vibrations at various frequencies and amplitudes to simulate motor-generated vibrations and other operational scenarios.
- Outcome: Ensure the chassis can effectively dampen vibrations and avoid resonance or structural fatigue.

preliminary testing plan

This section outlines the testing plan for the chassis of the hyperloop pod, ensuring its structural integrity and stability under various loads and conditions.

Static Load Testing

- Method: Securely mount the chassis at the suspension mounting holes.
- Loading: Apply a static load equivalent to twice the weight of the finished pod.
- Duration: Maintain the load for a predetermined period to assess the structural integrity.
- Measurement: Monitor for deformation or failure.

Dynamic Load Testing

- Method: Simulate dynamic forces experienced during operation.
- Loading: Apply forces to replicate acceleration, braking, and cornering.
- Duration: Perform over various speeds and conditions.
- Measurement: Record deflection and structural response.

Bending Stress Test

- Method: Use a reference part made from the same material as the chassis panels.
- Loading: Incrementally apply force until failure.
- Measurement: Note the force applied and deformation at failure.
- Expected Result: Determine material's bending strength and ductility.

Vibration Testing

- Method: Subject chassis to controlled vibrations across frequencies.
- Loading: Simulate operational vibrations.
- Duration: Extend testing for durability assessment.
- Measurement: Assess chassis damping and response to vibrations.
- Expected Result: Ensure chassis can maintain integrity under vibration.

Expected Results The chassis is expected to demonstrate stability and maintain structural integrity under static and dynamic loads. The bending stress test will confirm the material's properties, while vibration testing will validate damping capabilities. Through this comprehensive testing, the chassis will be proven to meet rigorous quality and safety standards, crucial for the hyperloop pod's performance.

2.3 Suspension

2.3.1 Introduction

Overview of the System

The front and rear double wishbone suspension system serves as a critical component within our Hyperloop pod, aimed at delivering a comfortable and stable ride experience. At its core lies the circular knuckle, meticulously designed to accommodate essential parts like bearings, retaining rings, and shafts. This central hub enables smooth vertical movement of the suspension, absorbing track imperfections for a seamless ride. Wishbones attached to the knuckle control suspension motion, featuring specialized bearings to maintain precise alignment. Dampeners directly connected to the knuckle assembly absorb shocks and vibrations, enhancing responsiveness to terrain changes. Additionally, a linkage mechanism minimizes lateral movement, ensuring stability, especially during high-speed travel. Integration with the chassis is facilitated by high-performance bearings, allowing for articulation and load transfer.

Requirements and Constraints

The suspension system must meet stringent requirements to ensure optimal performance and safety. It must provide exceptional ride quality, stability, and control throughout the journey, from acceleration to high-speed cruising. Constraints include optimizing weight distribution and reducing unsprung mass to enhance handling dynamics. The system must also minimize lateral sway and maintain course stability under demanding conditions. Incorporation of specialized bearings like the Female Wiebel Bearing further enhances stability and control. Meticulous engineering is essential to meet these requirements while adhering to space, weight, and durability constraints inherent to Hyperloop pod design.

2.3.2 Subsystem Overview

Explanation of Subsystem Concepts

Control Arms: The control arms are the primary components of the double wishbone suspension system, forming the distinctive "double wishbone" shape. These arms connect the Knuckle to the vehicle's chassis, with one arm positioned above and another below the wheel. They work together to control the wheel's vertical movement and maintain stability. This configuration allows the control arms to absorb bumps and shocks from the road while providing precise control over the wheel's motion.

Shock Absorbers (Dampers): Shock absorbers control the rate of compression and expansion of the springs, damping the oscillations of the suspension system caused by road imperfections. Shock absorbers play a crucial role in enhancing stability, comfort, and control by minimizing bounce and sway.

2.3.3 Theoretical Concepts

Detailed Explanation of Theoretical and Physical Principles

Theoretical Principles:

1. Independent Suspension:

   A fundamental theoretical principle underlying the double wishbone suspension is the provision of independent movement for each wheel. By decoupling the motion of one wheel from the other, this system ensures that disturbances affecting one wheel do not directly impact the other. This independence is crucial for maintaining optimal traction, stability, and comfort, particularly when navigating uneven terrain or cornering at high speeds. With independent suspension, variations in road surface or cornering forces can be effectively managed, enhancing overall vehicle dynamics.

2. Controlled Wheel Movement:

   The design of the wishbone-shaped control arms serves to control the movement of the wheel in multiple directions. These arms dictate the wheel's motion both vertically, for absorbing bumps and shocks, and horizontally, for steering input and stability. By strategically positioning and shaping the control arms, engineers can tailor the suspension's response to different driving conditions, ensuring precise handling and ride quality. This controlled movement allows for optimized wheel alignment, minimizing tire wear and maximizing grip, leading to improved overall performance and safety.

Physical Principles:

1. Shock Absorption:

   Shock absorption is a primary physical principle at work in a double wishbone suspension system. When the wheel encounters bumps or irregularities on the road surface, the suspension compresses and decompresses to absorb the impact. This process involves the coordinated action of the control arms and the shock absorbers (typically coilover or strut-type). The control arms guide the wheel's vertical movement, while the shock absorbers dampen the oscillations generated by road disturbances. Together, they mitigate the transmission of vibrations and shocks to the vehicle's chassis, providing occupants with a smoother and more comfortable ride experience.

2. Load Distribution and Handling:

   Load distribution and handling are essential physical principles influenced by the double wishbone suspension design. By distributing the vehicle's weight more evenly across all four wheels, this suspension system enhances traction and stability, especially during acceleration, braking, and cornering maneuvers. The geometry of the control arms plays a critical role in determining the vehicle's handling characteristics. Optimal geometry helps manage weight transfer during dynamic driving situations, ensuring responsive steering, minimal body roll, and enhanced cornering ability. Additionally, the precise control over wheel movement provided by the double wishbone setup contributes to predictable and balanced handling, promoting driver confidence and safety on the road.

Use of Free Body Diagrams for Load Cases

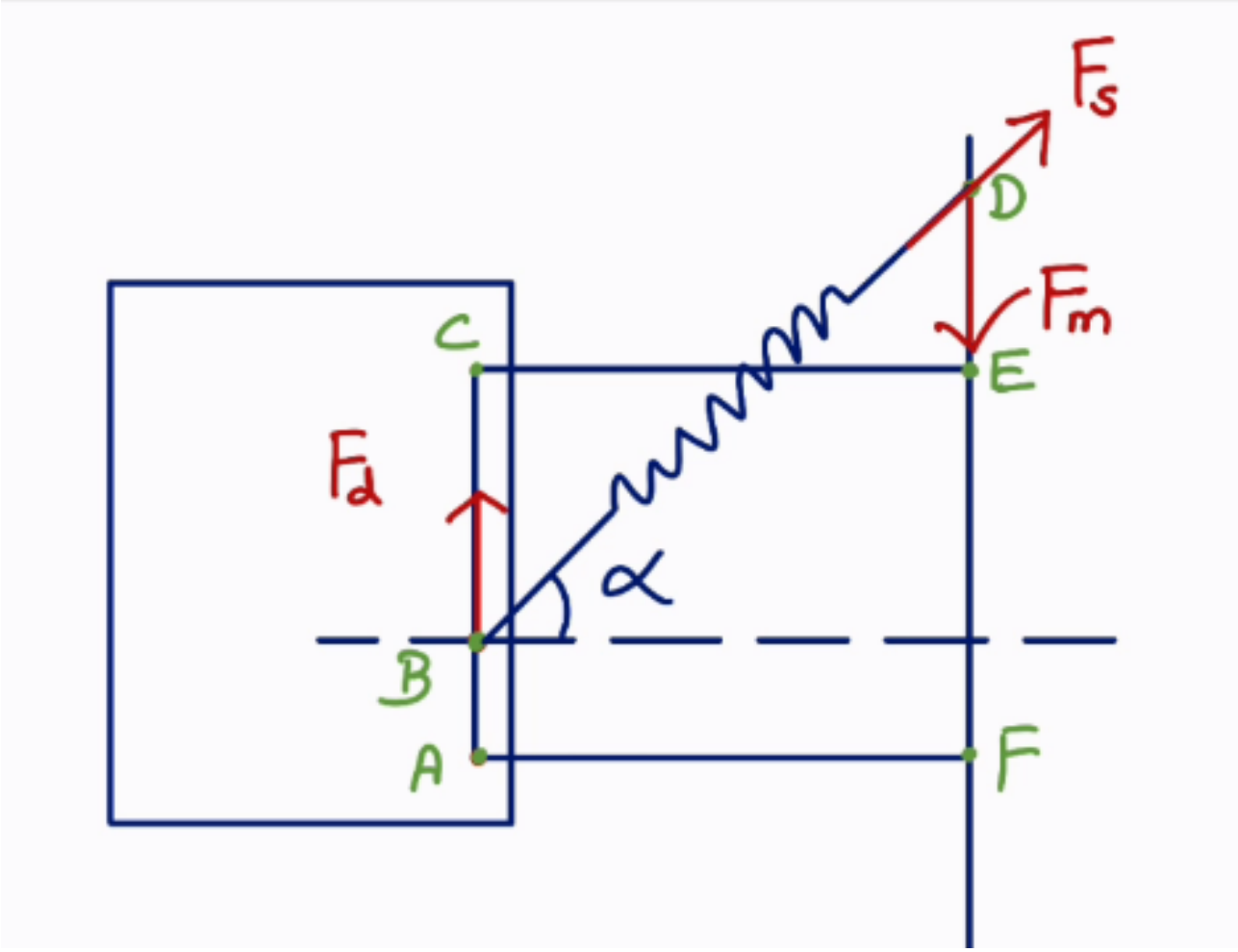

Figure 2.6: Caption for the image.

1. Fs:	Force of Shock Absorber
2. Fd:	Force due to disturbances
3. Fm:	Force to weight of the Chassis
4.α :	Horizontal angle of the Shock Absorber
5. CE:	Upper Wishbone
6. AF:	Lower wishbone
7. AC:	Knuckle

2.3.4 Design Process and Appearance

Presentation of CAD Models and Technical Drawings

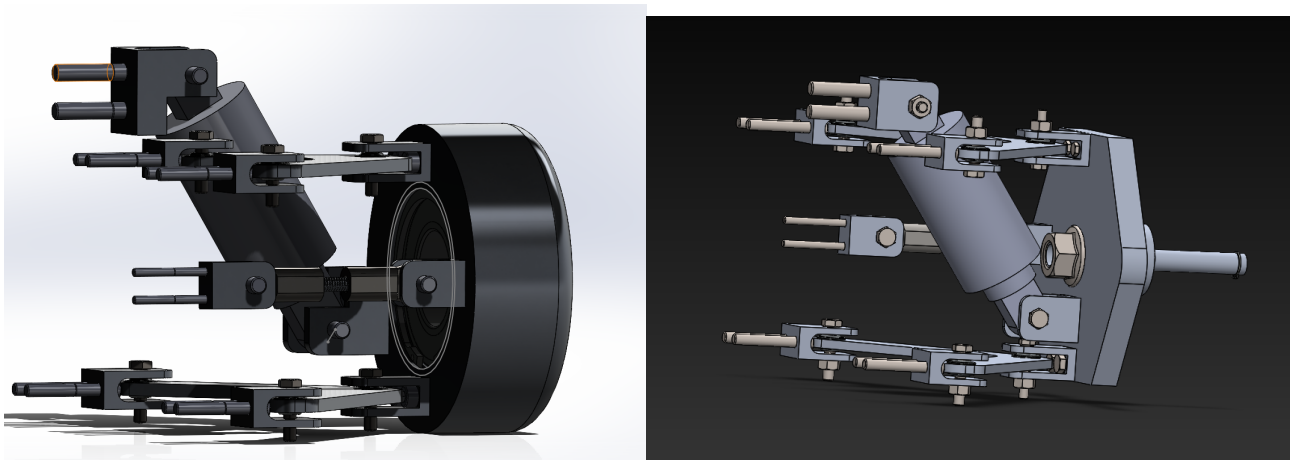

(a) Caption for the first image.

(b) Caption for the second image.

Justification of Material Selection

- High Strength-to-Weight Ratio: Utilizing Alloy 6061 would help reduce the overall weight of your suspension components while maintaining the necessary strength. This can improve the performance of your vehicle by reducing unsprung mass, which enhances handling, responsiveness, and fuel efficiency.
- Corrosion Resistance: The corrosion resistance of Alloy 6061 ensures the longevity and durability of your suspension components, especially considering the exposure to various environmental conditions and road debris that they may experience.
- Weldability and Formability: Alloy 6061's weldability and formability allow for the fabrication of complex and precisely shaped suspension components. This flexibility in manufacturing processes can help optimize the design of your suspension system for improved performance and reliability.
- Heat Treatability: Heat treatability provides the opportunity to enhance specific mechanical properties of your suspension components, such as strength and hardness. This can be particularly useful for critical components that undergo significant loads or stress during operation.

- Cost-Effectiveness: Alloy 6061 offers a cost-effective solution for your suspension system without compromising on quality or performance. This ensures that you can achieve your desired suspension characteristics while keeping manufacturing costs within budget.
- Recyclability: The recyclability of Alloy 6061 aligns with sustainability efforts and reduces environmental impact. Using a recyclable material for your suspension components contributes to the overall eco-friendliness of your vehicle's design.

Presentation of Material Properties

Table 2.2: Properties of Alloy 6061

Property	Value
Yield Strength	35 ksi (240 MPa)
Elongation at Break	10%
Fatigue Strength	96 MPa (14×10^3 psi)
Brinell Hardness	93
Young's Modulus	69 GPa (10×10^6 psi)
Thermal Conductivity	167 W/m·K
Melting Point	582°C (1080°F)
Heat Treating	Solution heat-treated (6061-W)

Presentation of Finite Element Method (FEM) Results

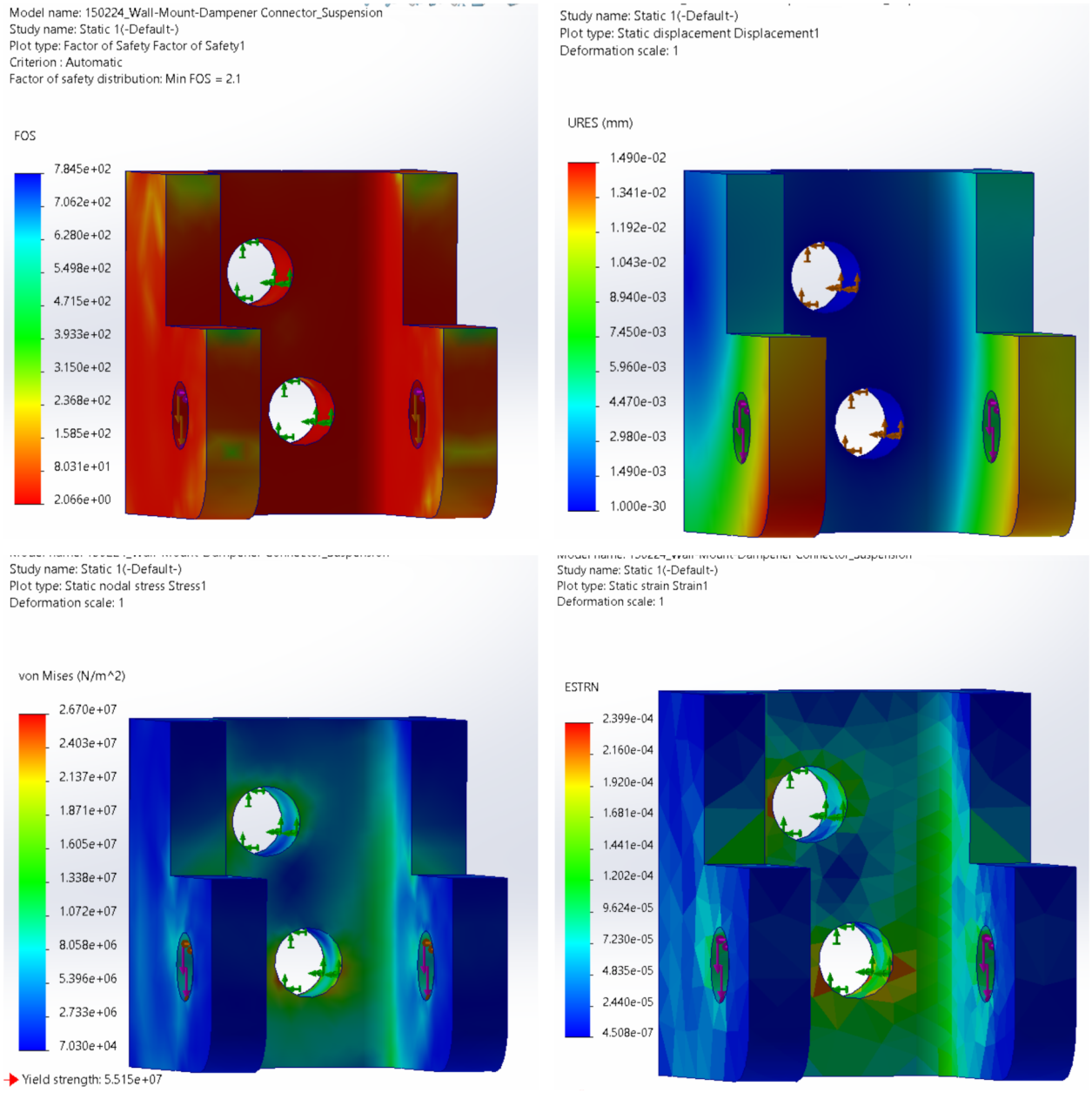

Figure 2.8: Caption for the image.

Table 2.3: Mesh Information - Details

Parameter	Value
Total Nodes	7097
Total Elements	4125
Maximum Aspect Ratio	6.3707
% of Elements with Aspect Ratio < 3	99.2

This study presents a Finite Element Analysis (FEA) conducted to evaluate the structural integrity and performance of the shock absorber mounting configuration on the knuckle of a rear double

wishbone suspension system. The primary objective was to assess the adequacy of the mounting design in withstanding applied forces and ensuring safety during operation. Initial simulations revealed areas of concern regarding the thickness of the mounting, prompting adjustments to the design parameters. Subsequent iterations were carried out to optimize the configuration, resulting in a revised model with enhanced strength characteristics. Through comprehensive analysis, a safety factor of 2 was achieved, indicating satisfactory resistance to anticipated loads. The findings of this study contribute to the understanding of structural behavior in automotive suspension systems and inform design improvements for enhanced performance and reliability (see Figure ??).

2.3.5 Manufacturing Process

Compilation of Parts List

Table 2.4: Components and Manufacturing Details

Component	Number	Mass [kg]	Size [mm]	Material	Manufacturing process	In-house/Outsourced
Rear Wheels	x2	-	ϕ 200 x 155	Aluminum Alloy 6061	In-house	In-house
Front Wheels	x2	-	ϕ 200 x 50	Galvanized Steel	Rollenplus.de	Outsourced
Rear Knuckle	x2	1.473	ϕ 145 x 52	Aluminum Alloy 6061	In-house	In-house
Cylindrical Roller Bearing Rear Knuckle	x4	-	ϕ 85 x 18.6	100Cr6	Outsourced	Outsourced
Retaining Ring DIN 472	x4	-	ϕ 85	Spring Steel	Mädler	Outsourced
Rear Upper Wishbone	x2	0.08896	119 x 102 x 6	Aluminum Alloy 6061	In-house	In-house
Rear Lower Wishbone	x2	0.1255	224 x 102 x 6	Aluminum Alloy 6061	In-house	In-house
Shock Absorber	x4	-	ϕ 45 x 150	-	XLC	Outsourced
Wishbone Wall Mount	x16	0.02441	36 x 30 x 18	Aluminum Alloy 6061	In-house	In-house
Knuckle Wishbone Mount	x8	0.02055	37 x 25 x 18	Aluminum Alloy 6061	In-house	In-house
Rear Shock Absorber Mounts	x4	0.05583	40 x 40 x 35	Aluminum Alloy 6061	In-house	In-house
Linkage Mounts	x8	0.0135	31.75 x 22 x 18	Aluminum Alloy 6061	In-house	In-house
Female Rod End Bearing	x8	-	47 x 16 x 14	Stainless Steel 1.4301	Mädler	Outsourced
Linkage Connecting Rod	x4	0.0032	ϕ 7 x 43	Aluminum Alloy 6061	In-house	In-house
Uni Ball Bearings	x24	-	ϕ 16 x 9	100Cr6	Mädler	Outsourced
Front Wheel Hub	x2	0.10959	ϕ 40 x 115	Aluminum Alloy 6061	In-house	In-house
Front Wishbones	x2	0.09553	224 x 102 x 6	Aluminum Alloy 6061	In-house	In-house
Front Knuckle	x2	0.65721	ϕ 160 x 15	Aluminum Alloy 6061	In-house	In-house
Front Shock Absorber Mounts	x4	0.01952	36 x 32 x 28	Aluminum Alloy 6061	In-house	In-house
Retaining Ring DIN 471	x2	-	ϕ 11	Spring Steel	Mädler	Outsourced

Description of Efforts for Realistic Manufacturability

Efforts for realistic manufacturability focus on optimizing production processes for critical suspension components, ensuring precision, reliability, and cost-effectiveness. This includes employing advanced manufacturing techniques and methodologies tailored to specific components, enhancing both efficiency and quality throughout the production process.

Explanation of Manufacturing Techniques

Knuckle Manufacturing: For the knuckle manufacturing process, a combination of water jet spray technology and CNC machining will be employed to ensure precise fabrication of critical features. The main hole for the shaft will be created using water jet spray technology, guaranteeing accuracy and efficiency in alignment and fitment. Additionally, advanced CNC machining will be utilized for creating internal grooves within the knuckle to accommodate the cylindrical roller bearings, ensuring precise dimensions and tolerances for proper seating and functionality of components.

Wishbone Manufacturing: Wishbones will be manufactured utilizing water jet spray technology, allowing for precise cutting of materials and efficient production. This ensures uniformity and consistency in the manufacturing process, resulting in high-quality wishbones that meet strict performance standards.

Linkage Rod Manufacturing: The linkage rod will undergo precision threading using a lathe machine, ensuring accurate fitment and functionality within the suspension system. This process guarantees precise dimensions and threading specifications, essential for seamless integration and optimal performance.

Mountings: Mountings on the knuckle assembly will be created using CNC machining, ensuring precise positioning and attachment of suspension components such as wishbones and shock absorbers. Additionally, the cylindrical roller bearings, facilitating specific movement within the knuckle, will be press-fitted to ensure secure placement and alignment. This method ensures stability and longevity within the suspension system.

2.3.6 Integration Process

Explanation of Integration with Other Subsystems

Integration with Other Subsystems: Integration with other subsystems is essential for ensuring the seamless operation and optimal performance of the suspension system within the overall vehicle architecture. In our case, integration with the propulsion system has been a key focus, particularly due to the presence of a shaft in the suspension design. This integration involves several considerations, including the offset positioning of the shock absorber to accommodate the shaft.

Shaft Integration: The presence of a shaft within the suspension system necessitates careful consideration to ensure compatibility with other vehicle subsystems, particularly the propulsion system. The shaft may be part of the drivetrain, connecting the engine or motor to the wheels for propulsion. Integration with the suspension requires accommodating the shaft's presence without compromising the functionality or performance of either system.

Offset Shock Absorber Positioning: To accommodate the shaft within the suspension assembly, the positioning of the shock absorber may need to be offset from its conventional location. This offset positioning ensures clearance between the shock absorber and the shaft, preventing interference and maintaining the integrity of both systems. By strategically adjusting the shock absorber position, we ensure optimal functionality of the suspension while accommodating the requirements of the propulsion system.

Integration with Braking System: In addition to integration with the propulsion system, seamless integration with the braking system is vital for overall vehicle performance and safety. Specifically, considerations have been made to ensure that the braking pads remain 7mm below the track surface for effective braking. This requirement has been addressed by utilizing an adjustable shock absorber design. By adjusting the shock absorber, we can precisely control the ride height of the vehicle, thereby maintaining the desired clearance for the braking system. This integration ensures that braking performance is not compromised and contributes to the overall safety and functionality of the vehicle.

By integrating the suspension system with the propulsion and braking systems, we achieve synergies that enhance overall vehicle performance, handling, and ride comfort. This integration

optimizes the utilization of space within the vehicle, maximizes efficiency, and ensures compatibility between critical subsystems. Additionally, it reflects our commitment to engineering solutions that prioritize functionality, reliability, and seamless operation across all vehicle systems.

2.4 Braking

The brake system in a vehicle is undeniably one of its most critical components, serving the vital function of controlling its speed and ensuring safe stops when necessary.

2.4.1 Overview

With various types of braking systems available:

- Mechanical Brake System
- Hydraulic Brake System
- Pneumatic Brake System
- Electromagnetic Brake System
- Electrical Brake System

Among these options, we have opted to implement the pneumatic braking system due to its simplicity in construction and its ability to provide a fail-safe mechanism through selection types. Pneumatic brakes offer reliable performance and can be well-suited for various vehicle applications, particularly those requiring robust and efficient braking capabilities.

Requirements and Constraints

In designing and implementing a vehicle's braking system or pod, careful attention is put on specific requirements and considerations. The complex design for the braking system of a pod depends largely on the maximum speed that can be achieved by the vehicle. Faster speeds call for finer brake parts to allow for proper and safe deceleration hence putting more emphasis on exactness in the system design. On top of this, knowing how much energy that is stored in it is vital to ensure safe braking operations. It is therefore important to discharge this energy properly during braking so as to avoid overheating, mechanical failure, and to preserve the reliability of this system.

Moreover, there are certain restrictions to be followed in order for the braking process to be effective. These also include handling efficiently static weight of the pod plus any additional loads experienced during operation. Also, it should be designed with respect to high vehicle speed when considering stopping power within a reasonable range for safety purposes of passengers. Knowledge about distance required stopping is very significant here; such that brakes are made so as they can safely cause deceleration within that distance hence preventing accidents from happening.By adhering meticulously to these requirements and constraints, a braking system can be designed and implemented effectively, ensuring the safety and optimal performance of the pod.

Concept

Our major objective is simple: to develop a brake system that can never fail, guaranteeing the highest level of dependability and safety. Important components of the system include actuators, springs, and a pneumatic system. The pre-compressed springs provide the majority of the braking force, while the pneumatic system and actuators help in controlling and holding them in position.

Because a pneumatic system reacts rapidly, which is essential for effective braking, we decided to retract the spring using it. Although we might think about utilizing electrical actuators, their cost is prohibitive and would necessitate a large budget adjustment for the entire pod. For the purposes of our project, the pneumatic technique makes the most sense.

2.5 Size, Components, and Appearance

Component	Number	Mass [g]	Size [mm]	Material	In-house/Outsourced
Main Spring	×16	3163.2	-	-	-
Brake Pad	×16	406.4	-	-	-
Pad Mounting Bracket	×4	2296.6	-	-	-
Big Actuator	×4	8868	-	-	-
Small Actuator	×8	2432	-	-	-
Tube 8mm	×5	-	-	-	-
Tube 6mm	×1.5	-	-	-	-
Tube 4mm	×1.5	-	-	-	-
Tube adapter 4-8	×6	-	-	-	-
Tube adapter 6-8	×4	-	-	-	-
X-connector 8mm	×2	-	-	-	-
T-connector 8mm	×10	-	-	-	-
Pressure regulator	×2	-	-	-	-
Pressure tank	×2	-	-	-	-
Pressure sensor	×8	-	-	-	-
Main valve	×2	-	-	-	-
Venting valve	×2	-	-	-	-
Manometer	×2	-	-	-	-
One way valve (adjustable)	×2	-	-	-	-
Proximity sensor	×4	-	-	-	-
Sensor adapter cable	×8	-	-	-	-
Light barrier	×2	-	-	-	-
Distance sensor	×2	-	-	-	-
Tank and PR adapter	×8	-	-	-	-
Main actuator adapter	×2	-	-	-	-
Side actuator adapter	×4	-	-	-	-
Manometer adapter	×4	-	-	-	-
Pressure sensor bracket	×8	-	-	-	-
One way valve bracket	×2	-	-	-	-
IO-Link® master USB	×1	-	-	-	-
IO-Link® master USB cable	×1	-	-	-	-
Blanking plug 8mm	×2	-	-	-	-
Muffler 8mm	×4	-	-	-	-
Multiple hose clamping bar	×2	-	-	-	-
Thread sealing tape	×1	-	-	-	-
Cable binders	×10	-	-	-	-
Brake Mounting	×2	-	-	-	-
Total Weight					

Table 2.5: Components and Manufacturing Details

2.5.1 Theoretical concepts

The sequence of events is triggered when you apply the brakes in the pneumatic brake system.The compressed springs are already in place and ready to go when the system is first supplied with compressed air.

The actuator piston is forced forward when you apply the brakes because the brakes send out a signal to release compressed air.Converting the compressed air's energy into mechanical energy to powers this movement.

In tandem, the pre-compressed spring expands and pushes the actuator piston further as the air pressure decreases. In order to create the necessary friction to slow down the vehicle, the expanding spring and the moving piston work together to bring the brake pad into contact with the braking surface.

2.5.2 Design Process and Appearance

Taking into account variables like weight, speed, and stopping distance is the first step in the system design process. According to the given parameters, the pod's target weight is 250 kg, and its top speed is 60 km/h. The pod must be able to be stopped with sufficient force by the braking mechanism. Currently, our solution satisfies this criteria by guaranteeing that the pod may stop fully within a 20.5 m.

CAD Models and Technical

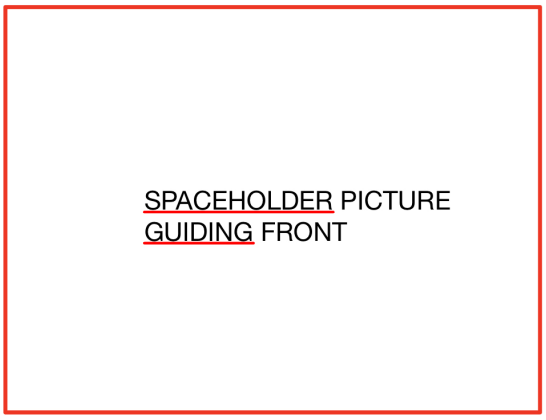

Figure 2.9: CAD Guiding Front

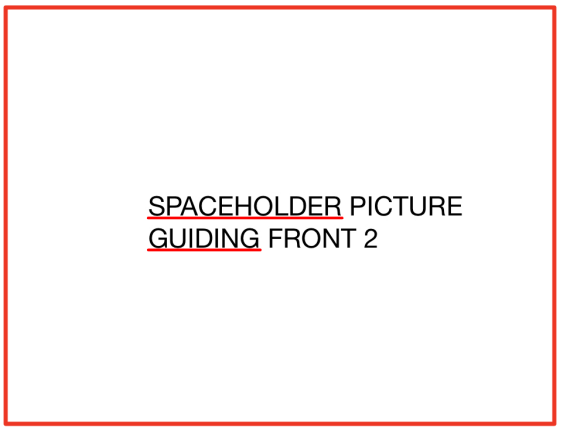

Figure 2.10: CAD Guiding Rear

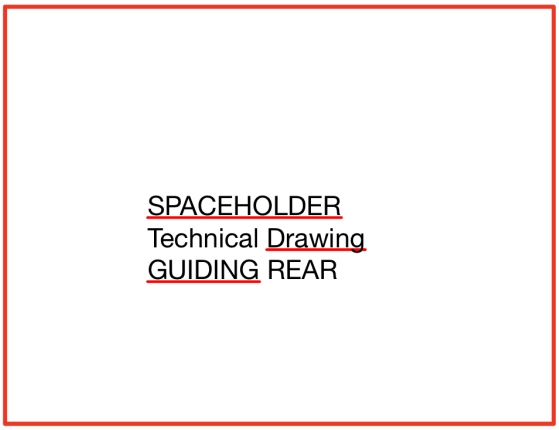

Figure 2.11: CAD Guiding Front #2

Figure 2.12: CAD Guiding Rear 2

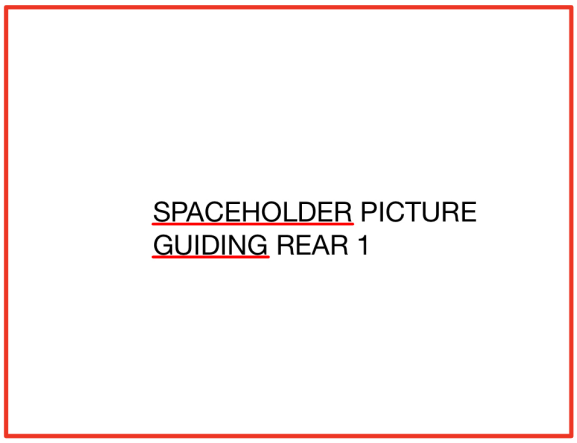

Figure 2.13: Technical Drawing Guiding Front

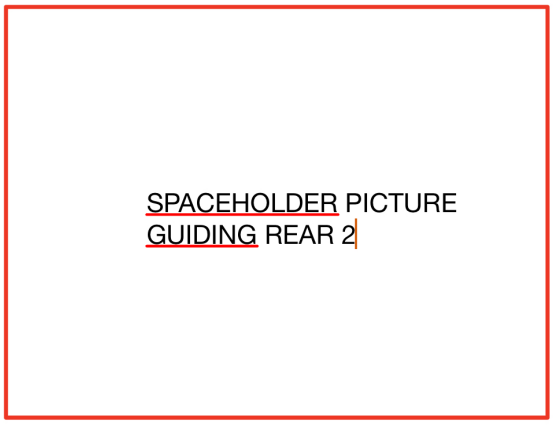

Figure 2.14: Technical Drawing Guiding Rear

Materials

To ensure maximum performance and longevity, the materials used for the subsystem components specifically, the small actuator mounting and the large brake mounting have been carefully chosen. The choice of plain carbon steel can be attributed to its superior mechanical properties, affordability, and suitability for its intended application. It's also simple to work with and shape during production, which lowers costs and promotes efficient production.

Because plain carbon steel is durable and resistant to corrosion, it can withstand extreme conditions and last for a very long time. It is very easy to weld, which makes assembly simpler.

Finding the ideal mix between strength, the lifespan, ease of manufacture, and cost-effectiveness was the main consideration in the selection of plain carbon steel for these components.

Design Rationale

The main goal of the braking system design is to use advanced design ideas and make sure the pod can stop completely within predetermined parameters.

The design's fundamental idea is to use springs to provide a fail-safe mechanism. Our goal in using springs is to create a braking mechanism that can operate even in the case of a leak or system failure. The unique part is how the actuators are used to keep the springs compressed by operating in reverse. This design element strengthens the system's fail-safe capability by guaranteeing that the pod can activate braking even in the event of a malfunction or physical damage. In conclusion, the braking system's creative use of actuators that operate in reverse and relying on springs are designed to promote safety and dependability. This method guarantees that even in

difficult situations, the pod can brake within predefined limits.

FEM Results

. Present FEM results for worst-case scenarios, including images and values.

Calculations:

- Kinetic Energy

For a pod with mass $m = 260$ kg and speed $v = 70$ km/h, kinetic energy is defined as

$$E_k = \frac{1}{2}mv^2$$

Substituting the given values:

$$E_k = 49151 \text{ J} \tag{2.1}$$

- Braking Force

To stop the pod within a certain distance, we must account for the work done to compensate for its kinetic energy. According to the principle of work, when an object moves against a force exerted on it, work is done. Specifically, if the object moves through a displacement d while experiencing a constant force F, the force performs an amount of work given by

$$W = F \cdot d$$

To find the force F exerted on the pod, given that the work done is $W = 49151$ J and the stopping distance is $d = 20$ m, we rearrange the formula:

$$F = \frac{W}{d}$$
$$\text{Braking force } F = 2457.6 \text{ N} \tag{2.2}$$

- Normal Force

To determine the required normal force exerted on the brake pads in order to achieve the necessary brake force, consideration must be given to the coefficient of friction ($\mu = 0.36$) between the brake pads and the track surface.

The required normal force (N) exerted on the brake pads can be calculated using the formula:

$$N = \frac{F}{\mu}$$
$$\text{N} = 6826.66 \text{ N} \tag{2.3}$$

where $F = 2457.6$ and $\mu = 0.36$.

The normal force per assembly, with consideration for two distinct assemblies, refers to the resultant force exerted perpendicular to the contact surfaces of each respective assembly.

$$\text{Normal force per assembly} = 3413.28 \text{ N} \tag{2.4}$$

- Spring Calculation

Given the parameters provided:

$$\begin{aligned}
\text{Resting length of the spring}(L_0) &= 187\,\text{mm} \\
\text{Spring constant}(k) &= 5.97\,\text{N/mm} \\
\text{Compressed length of the spring}(L_1) &= 94\,\text{mm} \\
\text{Actuator length}(L_{\text{actuator}}) &= 92\,\text{mm} \\
\text{Spring used in mounting}(L_{\text{mounting}}) &= 2\,\text{mm}
\end{aligned}$$

When the spring is compressed from its resting length to the compressed length:

$$\begin{aligned}
\text{Initial Force}(F_{\text{initial}}) &= k \times (L_0 - L_1) \\
&= 5.97 \times (187 - 94)\,\text{N} \\
&= 555.21\,\text{N}
\end{aligned}$$

Upon expansion of the spring to accommodate braking, extending to a length of 114 mm:

$$\begin{aligned}
\text{Force Required}(F_{\text{expansion}}) &= k \times (L_0 - L_{\text{braking}}) \\
&= 5.97 \times (187 - 114)\,\text{N} \\
&= 435.81\,\text{N}
\end{aligned}$$

Since each assembly utilizes 8 springs, the total force required for both assemblies is:

$$\begin{aligned}
\text{Total Force}(F_{\text{total}}) &= \text{Number of springs} \times F_{\text{expansion}} \\
\text{Total Force} &= 6972.96\,\text{N}
\end{aligned} \tag{2.5}$$

Considering the total normal force of 6826.66 N, it appears that the calculated force from the springs exceeds the total normal force, indicating that the system can function properly under these conditions.

- Actuator Force

To determine if the chosen actuators can effectively compress and hold the springs to meet the normal force requirement, we need to calculate the total force capacity provided by all actuators. Given that we have 2 big actuators and 4 small actuators, each with a capacity of 686 N (at 6 bar pressure), we can calculate the total force capacity for each assembly:

$$\text{Total force capacity} = 4116\,\text{N}$$

Comparing this with the required normal force of 3413.28 N, we can see that the total force capacity provided by the actuators exceeds the requirement. Therefore, the chosen actuators are sufficient to compress and hold the springs to achieve the desired normal force on the track surface.

- Actuator Pressure

Given that the system can handle pressures between 6 to 10 bar, with $P_1 = 6$ bar and $F_1 = 686$ N (as per the catalogue) where the actuator can exert a force of 686 N at 6 bar.

With 8 springs per assembly and a previously calculated compressed spring force of 555.21 N, the total compressed spring force per assembly is $8 \times 555.21 = 4441.68$ N.
Utilizing 6 actuators per assembly, the required force from each actuator is

$$F_2 = 740.28\,\text{N}.$$

Now, let's calculate the pressure required for the actuators to handle this force:

- Using the formula $F = P \times A$, where $F_1 = P_1 \times A$ and $F_2 = P_2 \times A$.

$$P_2 = \frac{P_1 \times F_2}{F_1}.$$

- Substituting the given values,

$$P_2 = 6.47\,\text{bar}. \tag{2.6}$$

Hence, the pressure required for the actuators to handle this condition is approximately 6.5 bar.

Mesh and Boundary Conditions

. Provide details on the type of mesh, boundary conditions, and Free Body Diagrams.

2.5.3 Manufacturing Process

Kindly consult Table 3.4 for reference.

We've taken steps to ensure that our braking system is more than just a concept and can be manufactured realistically.

Selecting Materials Which Are Easy to Use: The materials utilized for each component were selected based on their availability and convenience of production for the intended use. for instance, Carbon steel and other common metals, are chosen due to their easy production and wide availability.

Using Standard Parts: We made an effort to use components that are widely available and simple to assemble, such as tubes, connectors, and adapters. As a result, producers can assemble everything more easily and without the need for specialized tools.

Assembly Ease: The complete brake system's assembly has been taken into consideration. Parts are made to fit together easily, and assembly workers are assisted by clear labelling and instructions when needed.

2.5.4 Integration process

Assembling

Bolts will be used to firmly secure the main brake system to the chassis. Then, using specific mounts, small actuators will be fastened to the brake assembly.

Bolts will then be used to secure the aluminium brackets to the actuators. Before pressurizing the system, springs will be positioned between the metal brackets.

Assembly interaction

The longitudinal and lateral planes of the chassis must be securely fastened to the main mounting bracket. In in addition to providing structural support to the central section of the chassis, that connection will transmit forces to the chassis, resulting in the creation of a complete system.

2.5.5 Safety Considerations

Safety Factor

Selecting Strong Materials: Parts that make up pneumatic brakes, such as brake housings and valves, are made of hard materials such as steel and reinforced rubber These materials can withstand during braking.

To handle pressure safely: Air brake systems operate under high pressure, so the parts are designed to handle much higher pressures than they will actually experience during normal use This additional capability this ensures that the system remains safe even if pressure fluctuations or screws occur.

Passing safety tests: All parts in an air brake system go through rigorous tests to ensure they meet safety standards. These tests test things like how well the parts hold up under stress and whether they perform well under different conditions.

Backup system: Many brake systems have a built-in backup system. For example, if one part fails, there is usually another part that can take over, ensuring that the brakes remain functional in an emergency. In our case, springs are used to create a brake mechanism that can operate even in the event of a leak or system failure.

Worst-Case Scenarios

It can be dangerous to rely solely on air pressure in a standard pneumatic braking system without a fail-safe feature if the pressure drops unexpectedly or if there is a malfunction with the system.

Worst case scenario without Fail safe mechanism: This system only relies on air pressure. Leak of air or mechanical problem cause the air suddenly disappears, the brake might fail when needed. This makes accidents more likely.

Adding a Fail safe mechanism: if there is a problem with air pressure or in case might be drop, this fail safe feature turns on by itself. it makes sure the brakes keep working even if pressure drop.

2.5.6 FMEA Results Discussion

Risk Assessment

. Preliminary risk assessment for demonstration, transport, and lifting.

FMEA and Risk Mitigation

. Detail FMEA and describe risk mitigation measures.

Simulation Evidence

. Provide evidence of simulations validating theoretical assumptions.

2.5.7 Testing

Safety Procedures Documentation

Testing Procedures for Pneumatic Brake System

Pre-Test Inspection: Ensuring Braking component are properly attached and free from leaks. Check that the compressed springs are at right place and working properly.

Pressure Check: With use of pressure gauge to measure the air pressure in the system. Continue increase the pressure to the recommended operating level and check for any pressure drops before operating system.

Monitor the expansion of the spring: Verify the expansion of spring as the air pressure decreases.Check that the spring works in Simultaneously with the actuator piston to maintain proper braking force. Finally, Conduct a final inspection of all components of the system to ensure they remain in good condition.

Activate the Braking system by giving signal:Check how actuator piston react and check that it moves forward correctly. verify that the brake pad makes proper contact with the braking surface to create the friction that can enough to slow down the pod.

By applying emergency Brake Test: If we have to stop the vehicle in emergency situation,by conducting an emergency brake to check that it can able to quickly stop the pod.

Preliminary testing plan

As we discussed above preliminary testing plan for the pneumatic braking system involves several key tests to validate its functionality and performance.
The expected results include regularly pressure build-up, smoother movement of piston, spring expansion and enough friction of brake pad to slow down the vehicle and Safety precautions will be implemented throughout the testing process to ensure a safe environment and prevent any potential risk.

2.5.8 Additional considerations

Pneumatic Braking System:

Possible Failures: Brake systems can malfunction in a number of ways. it include malfunctioning , worn brake pads, pneumatic system failures, air leaks, worn brake pads or discs, electrical issues, mechanical damage and weather conditions. Regular inspection and maintenance are essential to ensure the system's reliability and safety.

Pressure Requirement: We are filling the pneumatic system with a pressure of 6.5 bar, well within the system's handling capacity, which ranges between 6 to 10 bar. To ensure that the pressure remains within safe limits, we are using a filling tank and pressure regulator. These components prevent the pressure from exceeding the specified limits and ensure the pneumatic system operates safely and effectively.

2.5.9 References

2.6 Eddy Current Braking

Due to unexpected changes in the team, we decided to halt the development of an eddy current brake, which would have served as an addition to our friction brake, which will conform to the standards of the competition after the redesign that is shown in the respective section.

2.7 Aerodynamics

2.7.1 Overview

The design of the Hyperloop pod aeroshell is meticulously crafted to optimize aerodynamic performance and ensure stability during high-speed travel. This section explores the key design considerations and features of the aeroshell subsystem, highlighting its role in reducing air resistance and enhancing the overall efficiency of the Hyperloop transportation system.

Requirements and Constraints

The Hyperloop pod aeroshell is required to fulfill several critical functions to ensure optimal performance of the transportation system. Firstly, it must minimize air resistance to facilitate smooth movement through the Hyperloop tube, thereby reducing energy consumption and increasing overall speed. Additionally, the aeroshell should enhance stability and control during acceleration, deceleration, and maneuvers, contributing to passenger comfort and safety. Furthermore, the design should incorporate features to manage airflow efficiently, preventing turbulence and ensuring a streamlined flow around the pod. Compliance with safety regulations and structural integrity are also paramount, ensuring the aeroshell can withstand operational stresses and environmental conditions encountered during Hyperloop travel.

Concept

The concept of the aeroshell subsystem revolves around maximizing aerodynamic efficiency while ensuring structural integrity and safety compliance. Inspired by proven aerodynamic principles, the aeroshell design prioritizes minimizing air resistance, enhancing stability, and facilitating controlled airflow. By incorporating features such as a streamlined front and rear configurations, the aeroshell optimizes performance while maintaining adherence to safety standards and regulatory requirements outlined in the Functional Design Description (FDD) for the Hyperloop competition.

Size, Components, and Appearance

. Include a table of materials, mass, dimensions, and other relevant factors.

2.7.2 Theoretical concepts

Theoretical understanding forms the backbone of our approach towards designing the aerodynamic components of the Hyperloop pod. In this section, we delve into the foundational concepts guiding our Computational Fluid Dynamics (CFD) simulations, specifically focusing on the utilization of the $k - \omega$ SST turbulence model.

Component	Number	Mass [kg]	Size [mm]	Material	Manufacturing process	In-house/ outsourced
Wheels	x8	1	100 x 50	Polyurethane	Injection molding	Outsourced
Axles	x8	0.2	10 x 90	Duplex Steel	Lathing	In-house
L-bracket 1	x16	0.1	20x30x50	Aluminium 7075	Milling	In-house
L-bracket 2	x8	0.2	30x40x60	Aluminium 7075	CNC	Outsourced
PART	AMOUNT	WEIGHT	SIZE	MATERIAL	PROCESS	SPONSORING

Table 2.6: Components and Manufacturing Details

Relevance of Turbulence Modeling

Turbulence plays a pivotal role in determining the flow characteristics around the Hyperloop pod as it travels through the tube. Traditional approaches relying solely on laminar flow assumptions are inadequate for capturing the complex flow phenomena at high speeds encountered in the Hyperloop environment. Therefore, turbulence modeling becomes indispensable for accurately predicting flow behavior, including boundary layer separation, vortex shedding, and wake formation.

Introduction to $k-\omega$ SST Turbulence Model

The $k-\omega$ SST (Shear-Stress Transport) turbulence model is a widely used approach in CFD simulations, renowned for its robustness and accuracy in capturing both near-wall and free-stream turbulence effects. This model combines the strengths of the $k-\omega$ and $k-\epsilon$ models, making it suitable for simulating a wide range of flow regimes, from boundary layers to separated flows.

Key Features of $k-\omega$ SST Model

The $k-\omega$ SST model resolves turbulent viscosity through two transport equations: one for turbulent kinetic energy (k) and the other for specific turbulence dissipation rate (ω). By incorporating wall functions and a low-Reynolds number correction, this model accurately predicts near-wall behavior while maintaining stability and computational efficiency. Additionally, the SST formulation seamlessly transitions between the near-wall region, where wall functions are utilized, and the outer flow region, where the standard $k-\omega$ model is applied.

The equations governing the $k-\omega$ SST model are as follows:

$$\frac{\partial(\rho k)}{\partial t}+\frac{\partial(\rho u_j k)}{\partial x_j}=P_k-\beta^*\rho\omega k+\frac{\partial}{\partial x_j}\left[\left(\mu+\frac{\mu_t}{\sigma_k}\right)\frac{\partial k}{\partial x_j}\right]$$
$$\frac{\partial(\rho\omega)}{\partial t}+\frac{\partial(\rho u_j \omega)}{\partial x_j}=P_\omega-\beta\rho\omega^2+\frac{\partial}{\partial x_j}\left[\left(\mu+\frac{\mu_t}{\sigma_\omega}\right)\frac{\partial \omega}{\partial x_j}\right]$$

where:

- P_k and P_ω are the production terms for k and ω respectively,
- β and β^* are constants,
- μ is the dynamic viscosity,
- μ_t is the turbulent viscosity,
- σ_k and σ_ω are the turbulent Prandtl numbers.

Aerodynamics Concepts: Lift and Drag

In aerodynamics, lift and drag are two fundamental forces that influence the motion of an object through a fluid. Lift is the force perpendicular to the relative motion of the fluid and the object, while drag is the force parallel to the relative motion.

The lift force (L) and drag force (D) can be calculated using the following formulas:

$$L = \frac{1}{2}\rho V^2 S C_L$$
$$D = \frac{1}{2}\rho V^2 S C_D$$

where:

- ρ is the fluid density,
- V is the velocity of the flow relative to the object,
- S is the reference area (such as wing area for an airfoil),
- C_L is the lift coefficient,
- C_D is the drag coefficient.

Key Fluid Mechanics Concepts

Several key principles from fluid mechanics are crucial for understanding aerodynamic behavior in CFD simulations:

- Reynolds Number (Re): A dimensionless quantity representing the ratio of inertial forces to viscous forces in the flow. It is defined as $Re = \frac{\rho V L}{\mu}$, where ρ is the fluid density, V is the velocity, L is a characteristic length (such as chord length for an airfoil), and μ is the dynamic viscosity.
- Boundary Layer: The thin layer of fluid adjacent to the surface of an object where viscous effects dominate. Understanding boundary layer behavior is essential for predicting aerodynamic drag and lift forces accurately.
- Turbulent Flow: Flow characterized by chaotic, irregular motion with fluctuations in velocity and pressure. Turbulent flow phenomena significantly affect drag, lift, and heat transfer in aerodynamic systems.

Unique Flow Regime

The Hyperloop pod operates within a distinctive flow regime characterized by very low Reynolds numbers (Re) and high Mach numbers (Ma). At low Reynolds numbers ($Re < 10^6$), viscous effects dominate, resulting in laminar flow over most of the aeroshell surface. High Mach numbers ($Ma > 0.3$) introduce compressibility effects, necessitating careful consideration of shock wave formation and drag rise. The interplay between these factors significantly influences the aerodynamic performance of the pod.

Boundary Layer Control

Effective boundary layer control is paramount for optimizing the aerodynamic efficiency of the pod. Transition delay techniques, such as passive and active boundary layer control, are employed to mitigate boundary layer separation and delay the onset of turbulent flow. Shaping the aeroshell to promote laminar-to-turbulent transition further upstream helps maintain attached flow and reduce drag. Additionally, employing boundary layer suction or blowing can manipulate flow separation points, enhancing overall aerodynamic performance.

Kantrowitz Limit

The Kantrowitz limit poses a critical challenge in the design of the Hyperloop pod aeroshell. Near this limit, where the pod's diameter approaches half the diameter of the tube, compressibility effects become significant. As the pod approaches transonic speeds, shock waves form, leading to increased drag and potential instability. Mitigating the adverse effects of the Kantrowitz limit requires careful shaping of the aeroshell to minimize wave drag and reduce perturbations in the flow field.

Meshing in CFD Simulations

Meshing, or grid generation, is a crucial step in CFD simulations that involves dividing the computational domain into discrete elements or cells. A well-structured mesh ensures accurate representation of flow physics while minimizing computational cost. For our Hyperloop pod simulations, a structured meshing approach is adopted to ensure optimal grid quality and resolution in critical flow regions.

Finite Element Method (FEM)

The Finite Element Method (FEM) is a numerical technique used to solve partial differential equations governing physical phenomena, such as fluid flow and structural mechanics. In the context of CFD simulations, FEM is employed to discretize the governing equations over the computational domain, enabling the solution of complex fluid flow problems. By dividing the domain into finite elements and employing appropriate interpolation functions, FEM facilitates the accurate approximation of flow variables within each element.

Integration into CFD Simulations

For our Hyperloop pod design, the $k-\omega$ SST turbulence model serves as a cornerstone in our CFD simulations. By accurately capturing turbulent flow phenomena, including laminar-to-turbulent transition

2.7.3 Results of Simulations

CFD Simulations

FEM Simulations

(To be done)The results of computational fluid dynamics (CFD) simulations provide valuable insights into the aerodynamic behavior of the Hyperloop pod aeroshell. Detailed analysis of flow patterns, pressure distributions, and drag coefficients derived from simulations inform design refinements and performance enhancements. The following subsection presents key findings and observations obtained from CFD simulations conducted on the Hyperloop pod aeroshell design.

2.7.4 Design Process and Appearance

CAD Models and Technical Drawings

. Present CAD models and technical drawings.

Figure 2.15: CAD shell Frontview

Figure 2.16: CAD shell sideview

Figure 2.17: CAD Shell back

Figure 2.18: CAD shell topview

Figure 2.19: CAD Shell drawing

Figure 2.20: CAD shell bottom

Materials

. Present and justify the selection of materials used in the subsystem . Provide relevant properties of the materials selected. The Aeroshell is constructed sustainably with natural basalt fibre

for biodegradability and superior tensile strenth. This iteration we used 3D printes molds, which enhance the design precision. Furthermore various safety features have been added to the Body, including using Polyester based Resins that are fire resistant.

Design Rationale

. Detail the design rationale behind the components of the infrastructure. . Provide a rationale for why the specific configuration has been chosen
The Hyperloop shell was designed in Autodesk Fusion 360. First we collected several information about optimal aerodynamic shell designs.To fit the chassis we went with a rounded rectangular form. The shell has smooth and regular surfaces for laminar airflow. Originally doors were planned for easy access to the battery. Due to time constraints we decided to implement a quick release mechanism so one is able to "take off" the whole shell and have access to the whole chassis. Furthermore the rear end is flattened to reduce the drag force on our pod.

FEM Results

. Present FEM results for worst-case scenarios, including images and values.

Calculations . Provide reasoning and the necessary calculations to justify the simulated loads.

Mesh and Boundary Conditions

. Provide details on the type of mesh, boundary conditions, and Free Body Diagrams.

2.7.5 Manufacturing Process

. Compile a parts list in tabular format, specifying in-house or outsourced production. .Describe what efforts have been made so that the designed part is realistically manufacturable.

Component	Number	Mass [kg]	Size [mm]	Material	Manufacturing process	In-house/ outsourced
Bed lift	x2	7	-	steel	-	Outsourced
Lamination bolt	x8	0,01	M6	stainless steel	-	Outsourced
Nuts	x8	0,0012	M6	alloyed steel	-	Outsourced
3D-Print	x1	-	-	-	-	Outsourced
Epoxidharz	x1	-	-	-	-	Outsorced
PART	AMOUNT	WEIGHT	SIZE	MATERIAL	PROCESS	SPONSORING

Table 2.7: Components and Manufacturing Details

The construction process for Fermions aeroshell involves a systematic approach to ensure the optimal integration of basalt fibers and polyester resin. Beginning with a detailed design and 3D model, the chosen shape, dimensions, and structural requirements are meticulously defined using Autodesk Fusion 360. To get the shape designed in CAD, we are 3D-printing our Shell. Following material selection a custom mold is prepared to reflect the rounded rectangular aeroshell geometry.
In preparation for the layup process, the mold undergoes surface treatment with a mold release agent to facilitate subsequent removal. Basalt fibers are then cut to specified lengths and strategically laid onto the mold, ensuring even distribution and coverage, particularly in areas with complex

shapes or anticipated high-stress points. The wet layup method is employed, involving the careful application of polyester resin to saturate and bond with the basalt fibers.
To consolidate the composite structure, a consolidation tool is utilized, eliminating air bubbles and enhancing the adhesion between the basalt fibers and the resin. The aeroshell is left to fully dry. Following a thorough curing process, the aeroshell is demolded with precision to prevent damage to the composite structure.
Post-demolding, excess material is trimmed, and meticulous finishing is conducted to achieve a smooth and aerodynamic surface. After the shell is cured and demoulded, the mountings will be fixed from the inside with layup. To give Fermion a modern look and therefore visualize the new and futuristic approach of the hyperloop system, the shell will be painted.

2.7.6 Integration process

Assembling

Preparation Phase: Firstly, we gather all the necessary components, such as the aeroshell, chassis, and lifting mechanism. We meticulously inspect each part, ensuring they're in optimal condition for assembly. If we spot any damaged or faulty components, we promptly replace them to avoid any issues during integration.

Assembly of Lifting Mechanism: Following the preparation phase, we carefully assemble the lifting mechanism according to the manufacturer's instructions. This involves constructing the hydraulic arms and triangular metal structure. Proper assembly is crucial for the smooth operation and safety of the lifting process.

Attachment to Chassis: Once the lifting mechanism is assembled, we securely attach it to the chassis. We make sure to create a firm and stable connection to support the weight of the aeroshell during lifting. Bolting the lifting mechanism securely to the chassis is vital for stability and safety.

Assembly interaction

Lifting the Aeroshell: With the lifting mechanism securely in place, we begin the process of lifting the aeroshell. We lift it evenly and cautiously to prevent any tilting or imbalance that could potentially damage the aeroshell. Careful operation of the lifting mechanism is essential for a safe and smooth lifting process.

Integration Phase: Once the aeroshell is lifted to the appropriate height, we carefully lower it onto the chassis. Alignment is critical at this stage to ensure proper fitting and performance. We verify that the aeroshell aligns correctly with the mounting points on the chassis.

Securing and Final Checks: After positioning the aeroshell on the chassis, we secure it using appropriate fasteners. We ensure these fasteners are tightened securely to firmly attach the aeroshell to the chassis. Conducting a thorough final inspection is crucial to confirm the secure attachment of the aeroshell and the proper functioning of the lifting mechanism.

Final Checks: In the final stage of the integration process, we conduct a comprehensive inspection. We check to ensure that the aeroshell is securely attached and that the lifting mechanism is functioning correctly. Any issues identified during these final checks are addressed promptly to ensure successful integration.

2.7.7 Safety Considerations

Safety Factor

. Discuss the safety factor applied to structural elements.

Various safety measures have been considered to minimize failures. Furthermore performing FEA ensures that our aeroshell can sustain High Shear Stresses. An assembly test was performed

to ensure violation of the keep out zones. As already mentioned in ”Materials”, the resins for the chosen composite are fire resistant.

Worst-Case Scenarios

. Discuss worst-case scenarios (e.g., worst-case braking deceleration) and what you plan to do to avoid or contain them.

1. Structural Failure:

Structural fatigue could result from manufacturing defects, material weaknesses or unforeseen stress factors. To avoid structural failure, we carefully selected materials with high fatigue resistance for constructing the aeroshell. (carbon fiber reinforced polymers)

2. High speed collision:

High speed collisions could occur when external objects penetrate the shell. The Aeroshell must be able to withstand the impact forces. Similar to the first point, we are using carefully selected materials.

3. Fire Incidents:

In the event of a fire within the system, the aeroshell ist designed to withstand high temperatures and prevent the spread of flames due to the fire resistant resins.

2.7.8 FMEA Results Discussion

Risk Assessment

. Preliminary risk assessment for demonstration, transport, and lifting.

FMEA and Risk Mitigation

. Detail FMEA and describe risk mitigation measures.

Simulation Evidence

. Provide evidence of simulations validating theoretical assumptions.

2.7.9 Testing

Safety Procedures Documentation

. Describe testing procedures.

preliminary testing plan

. Provide a preliminary testing plan, including methodology and expected results.

2.7.10 Additional considerations

. Additional considerations when writing the document for specific subsystems: Breaking, Pneumatic system, Aeroshell. i. Include CFD analyses for the conditions expected during the demonstration, and their results, covering values such as lift, drag, or moment coefficient. ii. If you plan on demonstrating inside a tube, include it in the CFD simulations. iii. In case the system uses high voltage, indicate how will the MIDs be shut off when the aeroshell is covering the pod

Traction System

3.1 Introduction

3.2 Propulsion

3.2.1 Overview

To accelerate our Hyperloopod we use our EMRAX 188 electric motor from last season. This delivers an output of 60 kW under high voltage and a maximum torque of 100 Nm. This torque gets transferred to a right-angle gearbox and from there is slid to the drive wheels via cardan joints.

Concept

The main goal of this system is to accelerate our pod with an acceleration of $5\,\mathrm{m/s^2}$. Since the given $100\,\mathrm{Nm}$ are not sufficient under an estimated total weight of $250\,\mathrm{kg}$, the drivetrain requires a gear ratio. Since an angular gearbox is installed anyway, it is easy to implement this criterion there. In order to maintain a relatively high top speed of the pod, this transmission ratio should be as close as possible. According to the formula

$$T_{\text{required}} = \frac{(m \cdot a + \frac{1}{2} \cdot \rho_{\text{air}} \cdot C_w \cdot A_{\text{Aeroshell}} \cdot v^2 + m \cdot g \cdot \cos(\Theta)) \cdot r}{\eta}$$

we know that we require at least around $170\,\mathrm{Nm}$ of torque to achieve this amount of acceleration. While the pod weight of $250\,\mathrm{kg}$ is only an estimate at the time of system design and we are always keen to get such complex parts from our partners, we opted for a $2:1$ ratio of a Mädler gearbox. With this gear ratio, a respectable top speed of $113\,\mathrm{km/h}$ is still possible. This is absolutely sufficient for our prototype, as we are still sticking to our basic idea: For low speeds and accelerations, we drive our hyperloop pod with a conventional wheel drive and for everything above that, the pod will hover with a linear induction motor which will be added in future prototypes. We believe that we can achieve an increase in efficiency in this way as permanent levitation is not necessary.

The transmitted torque must now be directed to the drive wheels in such a way that it is still possible to ensure a working suspension. For this, we use universal joints on both sides of the centered bevel gear. These also come from our partner Mädler and are connected to the bevel gear using in-house produced adapter shafts and feather keys. To finally connect the other ends of the shaft joints to the wheel, only one last shaft is missing. This is also fitted with a keyway on the joint side and a bolt circle on a flange on the wheel side. Now that the wheels are supplied with power, it is important to create sufficient rolling friction. To achieve this, Continental provides us with a rubber coating for our wheels.
Of course, this all has to be mounted into the chassis. For this, we use three different types of brackets beside the knuckles, where the wheelshafts are mounted: one for the motor, one for the motorshaft and two of the same kind, which carry everything between the shaft joints.

Size, Components, and Appearance

Table 3.4

Component	Number	Mass [kg]	Size [mm]	In-house/ outsourced
Motor	x1	7	$188 \times 188 \times 112$	Bought
Motorshaft	x1	0.4	$170 \times 83 \times 83$	Outsourced
Bevelgear z=20	x1	3	10×90	Bought
Bevelgear z=40	x1	9.6	$20 \times 30 \times 50$	Bought
Gearshaft Pressfitted	x1	0.3	$103 \times 40 \times 40$	Outsourced
Gearshaft bolted	x1	0.7	$106 \times 55 \times 55$	Outsourced
Shaft Joint	x2	4.1	$30 \times 40 \times 60$	Bought
Wheelshaft	x2	0.7	$138 \times 100 \times 100$	Outsourced
Wheel	x2	1.7	$200 \times 200 \times 155$	Outsourced

Table 3.1: Components

3.2.2 Design Process and Appearance

Motor

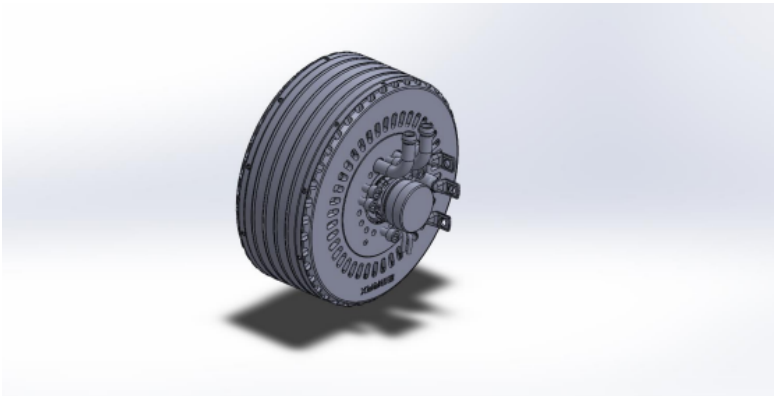

Figure 3.1: CAD of EMRAX 188

As previously mentioned, we are once again using our EMARX 188 electric motor from last season. You can find all the technical details in Table 3.27 .

Motorshaft

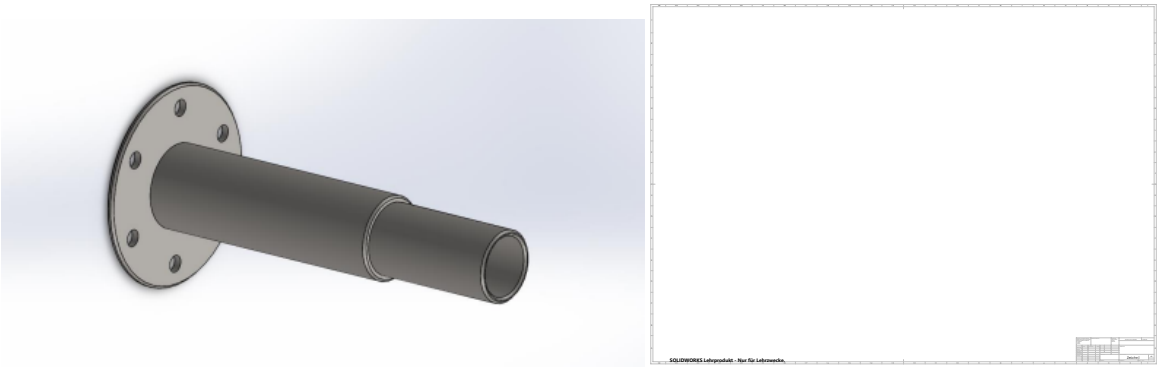

(a) CAD Render (b) Technical Drawing

Figure 3.2: Motor Bracket

Even though it is a heavy material, C45 steel provides adequate tensile strength to transmit torque from the motor to the gearbox or from the gearbox to the wheels. To maintain a relatively low weight for this part, it is hollow like all the other shafts. In Figure 3.3, you can now see the applied forces. The shaft is mounted on the motor at the screw holes of the flange (green). This means that the motor torque of 100 Nm (pink) acts up to the surface on which the bevel gear is pressed. The calculation of the contact pressure of 16.26 MPa is given by

$$p_{\text{contact}} = \frac{2 \cdot M \cdot S_r}{\pi \cdot D^2 \cdot l \cdot \mu}$$

In addition, there is a centrifugal force (blue) at maximum rotational speed of 6000 rpm.

Figure 3.3

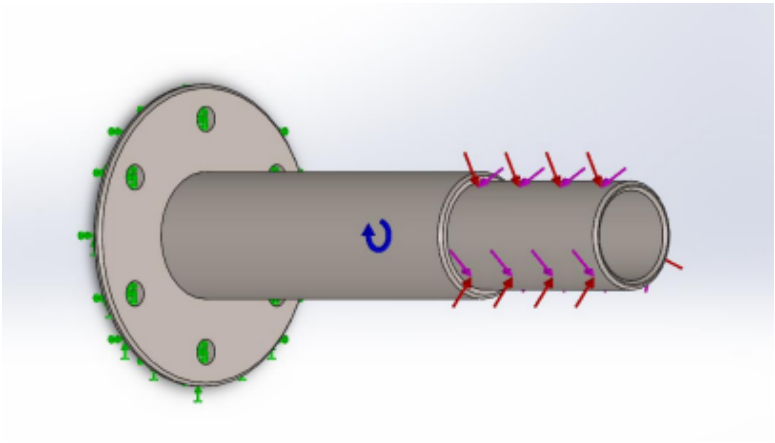

Figure 3.3: Forces acting on the Motorshaft

Bevel Gears

picture gearbox

The bevel gears with the article numbers 36736000 and 36736100 are our choice to fulfill the desired purpose. 36736000 offers spur gearing with 20 teeth. With a maximum permissible torque of 130 Nm, it can withstand the prevailing forces. The larger counterpart 36736100 therefore has twice as many teeth (40 teeth) and is designed for a maximum torque of 260 Nm.

Gearshafts

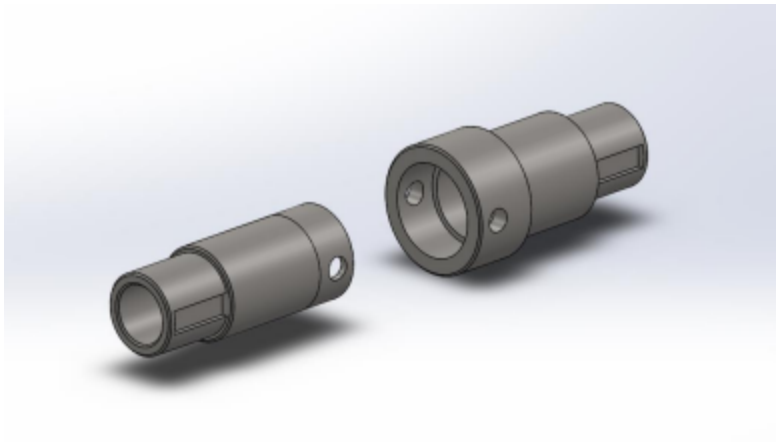

Figure 3.4

To be able to conduct the torque of the bevel gear, we have designed another shaft. This consists of two individual parts, one which is again pressed into the bevel gear and the other which is screwed onto the first part after pressing. The specifications of the initially acting shaft are as follows:

Figure 3.5

Figure 3.6

Fig.xx shows all the acting forces. For calculating the pressing force (red) we again use the formula for p_{contact} and get the result of 21.22 MPa. The higher torque of 200 Nm (pink) resulting from the gear ratio also acts on this surface and is transferred to the screw holes and keyway (green). A centrifugal force (blue) also acts on this part, but this has now been halved by the gear ratio and is therefore only based on 3000 rpm. Finally, we assume a bearing restraint (orange) at the shaft end to the shaft joint. The admissibility of this case is described in the paragraph on the shaft joint itself.

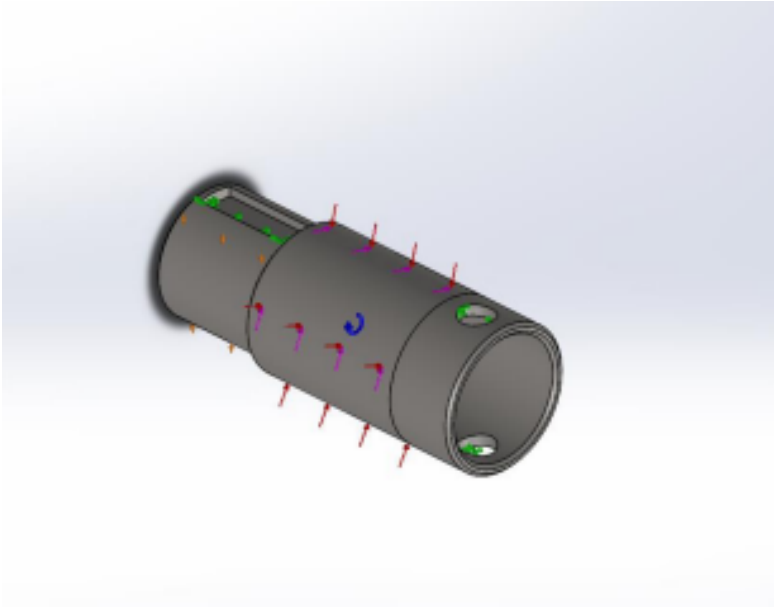

Figure 3.7: Forces acting on the pressfitted Gearshaft

The torque is now transferred to the second part of the gearshaft:

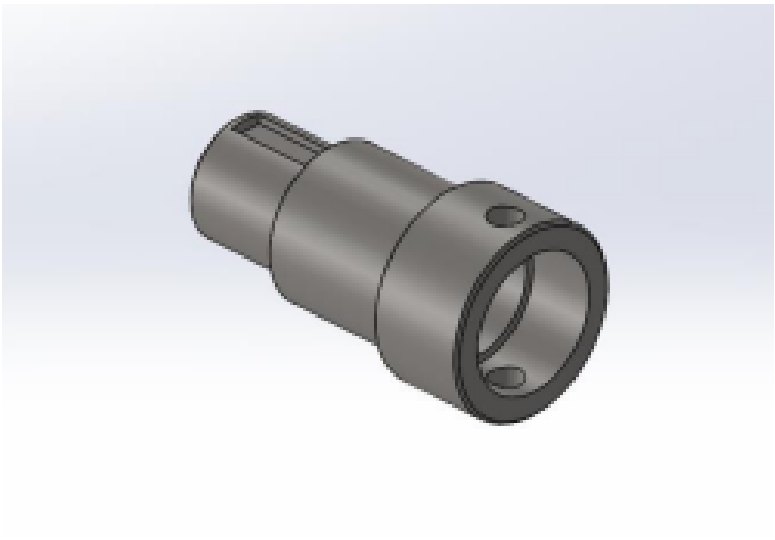

Figure 3.8

Figure 3.9

Fig.xx shows all the forces acting on this part. The two shafts are connected to each other at the screw holes (green). The centrifugal force (blue) acts as in the first shaft at 3000 rpm and the torque of 200 Nm (pink) up to the keyway. This end piece of the shaft is also simulated as a bearing (orange).

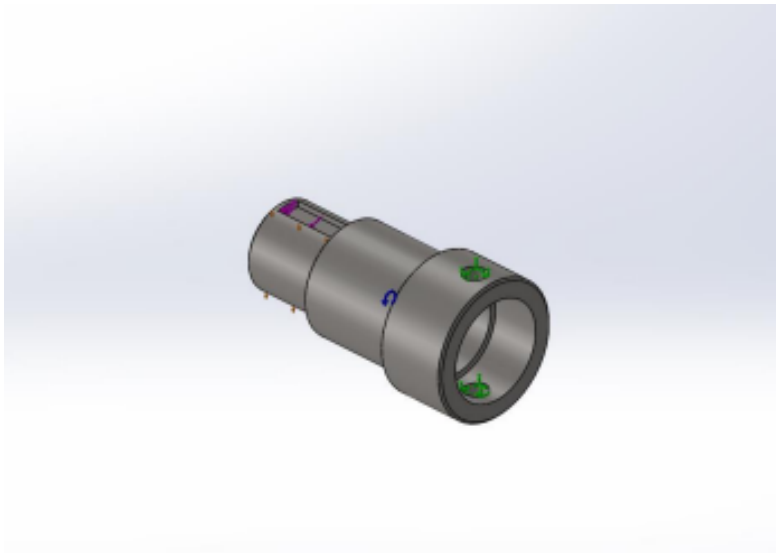

Figure 3.10: Forces acting on the bolted Gearshaft

Shaft Joints

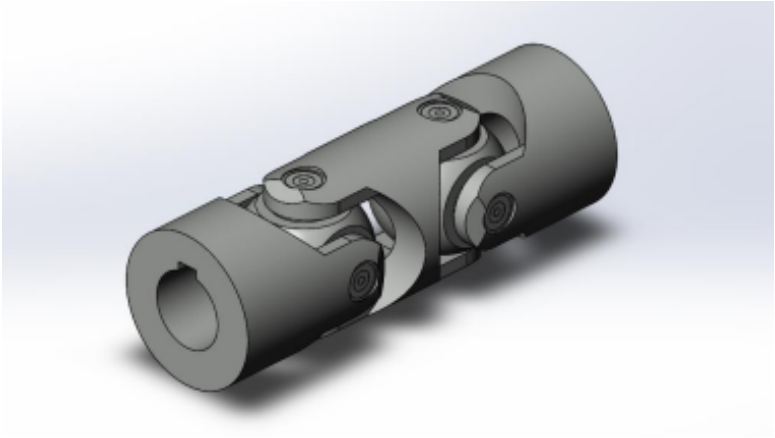

Figure 3.11

To enable the system to absorb shocks, we use cardan shafts on each side. This allows the wheels to move vertically independently of the rest of the pod. Our partner Mädler is once again supplying us with such complex parts. Item number 6 3167000N is a double universal joint which we install in our system. It has a keyway at both ends and is designed to transmit 202 Nm at 3000 rpm. These specifications are almost perfect for our drive power. We will mount the heart of our system at the ends of this joint adjacent to the gearbox. This is also the reason why a bearing is created at the respective ends in the simulations of the shafts because this bearing is also attached above the respective area. However, more on the bearing and attachment points will follow in the corresponding sections.

Wheelshafts

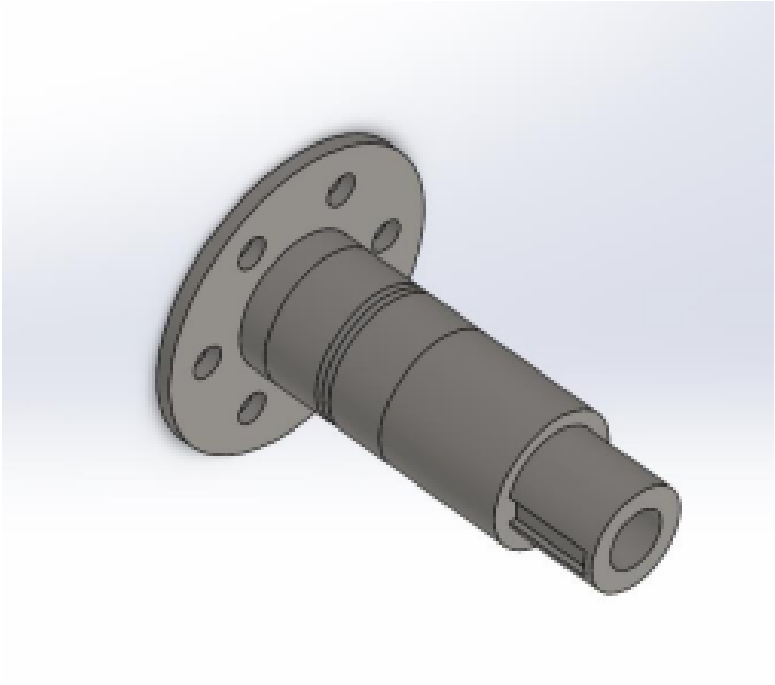

Figure 3.12

The wheel shafts provide the mounting point for the wheels. This is done by means of a bolt circle on a flange to ensure easy mounting and, if necessary, changing of the wheels. In this shaft,

Figure 3.13

the 200 Nm torque (pink) applied to the keyway is transmitted to the wheel over the entire surface of the flange. The centrifugal force (blue) is also generated again due to the 3000 rpm and this shaft is also mounted on bearings (orange) within the knuckles. You can find out more about this bearing in the suspension section. However, this shaft must be able to withstand the mass inertia of the wheel (red). This is calculated by $5/2 \times m_{\text{wheel}} \times a$

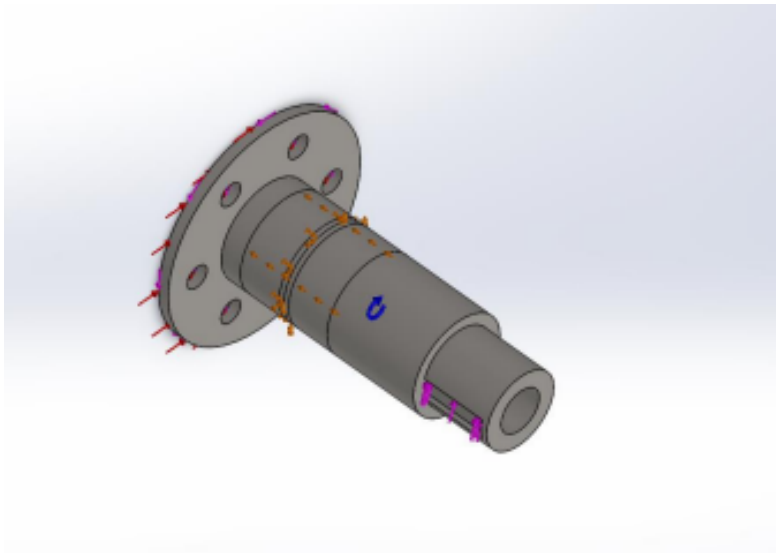

Figure 3.14: Forces acting on the wheelshaft

Wheels

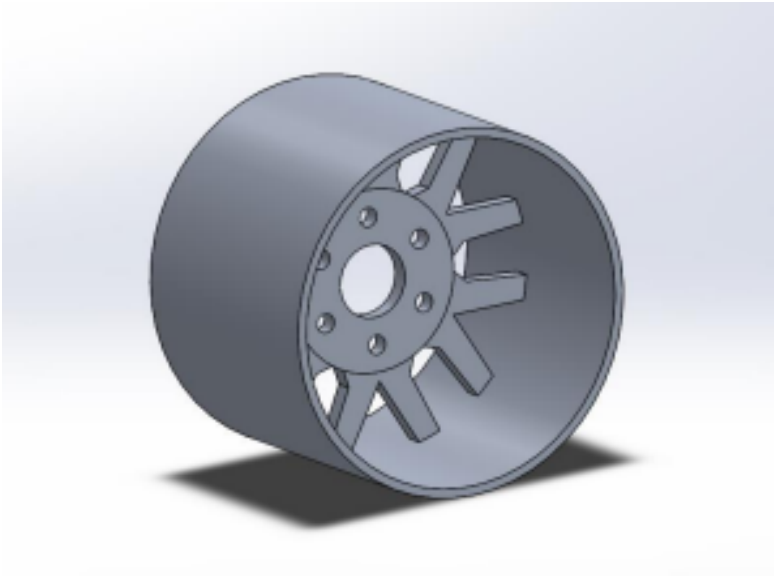

Figure 3.15

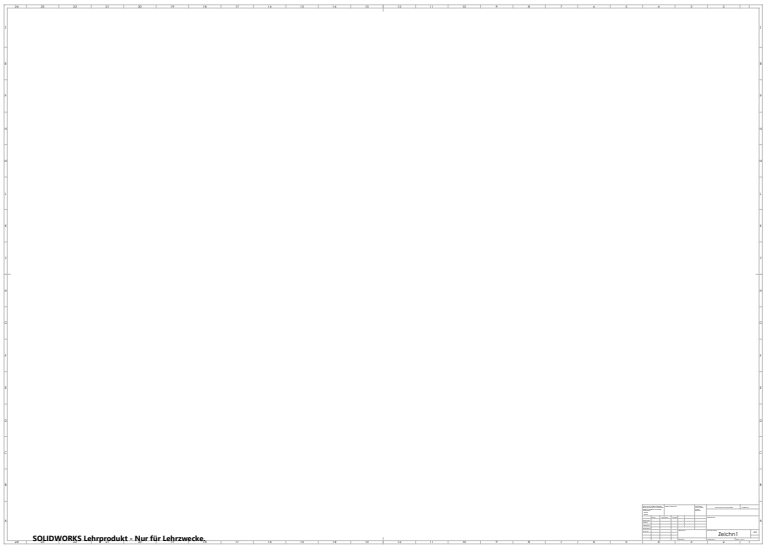

Figure 3.16

Finally, we transfer the torque (pink) to the wheels via the contact surface of the flange (green). The mass inertia of the wheel (red) $5/2 \times m_{\text{wheel}} \times a$, again the centrifugal force at 3000 rpm (blue) and the local pod weight of approximately 600 N (orange) also have an effect here. This weight, together with the rolling friction coefficient of the rubber cover, enables slip-free propulsion. We get this coefficient of 0,5099 by the formula

$$\frac{m \cdot a}{m \cdot g}$$

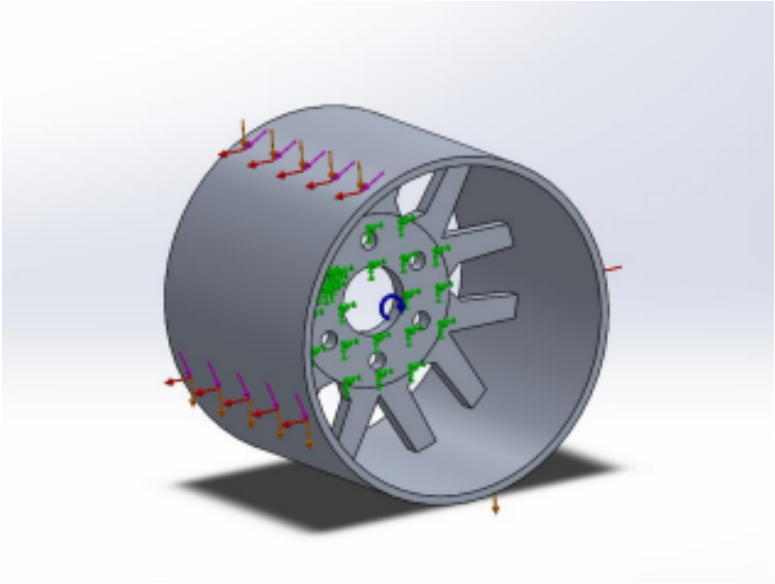

Figure 3.17: Forces acting on the wheels

Motorbracket

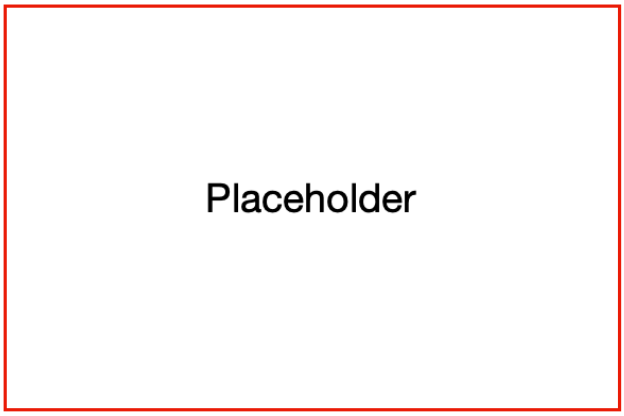

(a) CAD Render

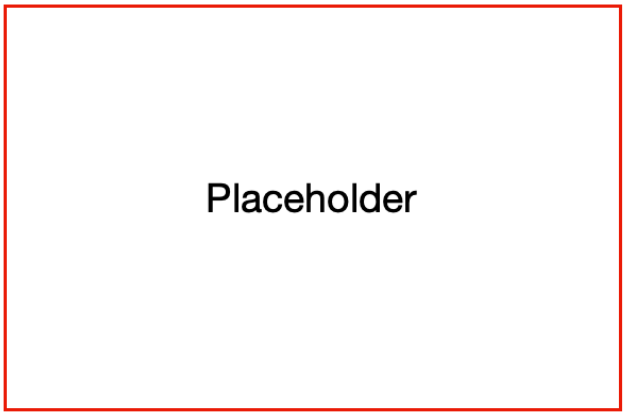

(b) Technical Drawing

Figure 3.18: Motor Bracket

Our motor is mounted in the chassis using a bracket. This contains all the holes for screws and other components that protrude to the rear. End plates with screw holes are welded to four arms to finally screw () them into the chassis. The torque () and the inertia of the motor () prevail at this bracket.

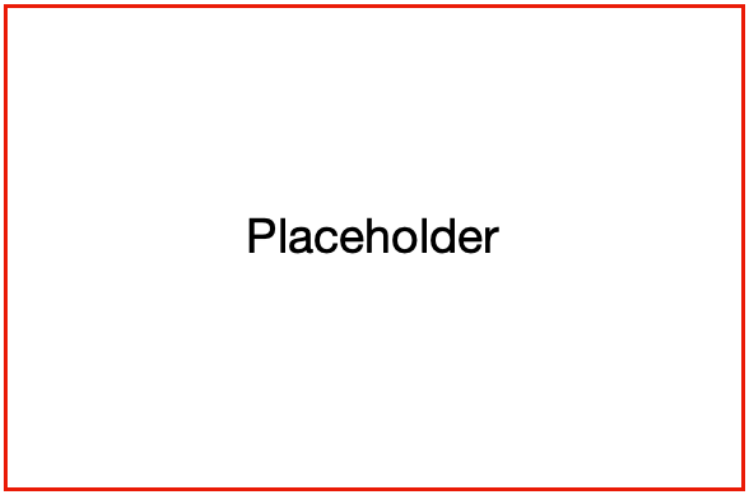

Figure 3.19: Forces acting on the motorbracket

Motorshaftbracket

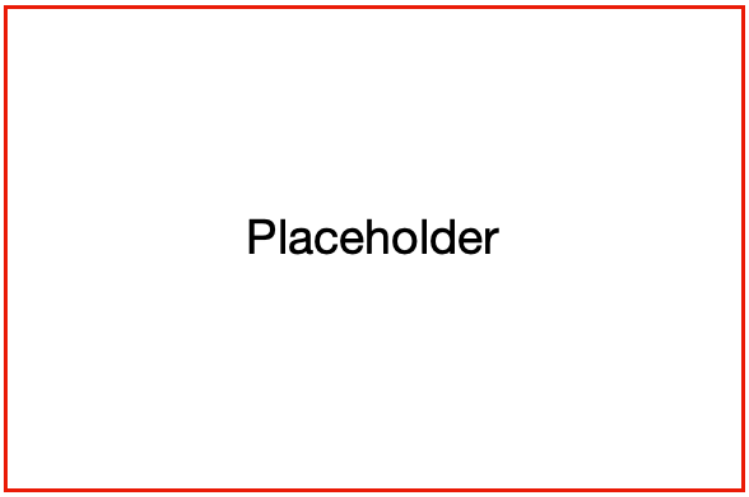

Figure 3.20

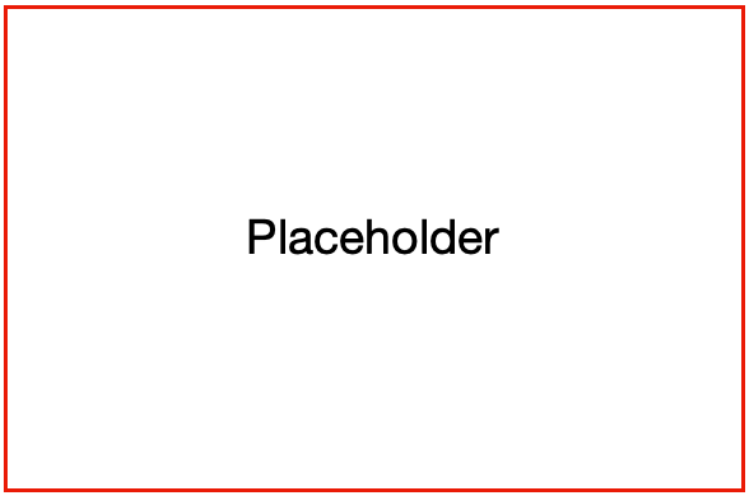

Figure 3.21

To finally support this first area of the drive system, we also support the shaft that protrudes from the motor. This is done using the CHDF35 flangebearing from Misumi. This bearing is finally integrated into the chassis by another bracket. Only the weight of the motor shaft (), its mass inertia and the wheight of the flangebearing () act on this bracket.

Bearinghouse

To provide sufficient support for the drive axle, we mount it at two points. For space reasons, we designed the bearinghouse ourselves. The weight of the axle (pink) acts on this bearinghouse at the respective point, as well as its mass moment of inertia (). This bearing shell is installed with screws (green) on another bracket in the chassis.

Bearingbracket

As already mentioned, the bearinghouses are mounted on additional brackets. Like the motor brackets, these brackets consist of a plate with screw holes () to which end plates are welded via which the component is installed in the chassis (). The same forces act on this bracket as on the bearinghouse with the weight of the bearinghouse itself ().

Materials

Component	Number	Mass [kg]	Total Mass [kg]	Material
Motor	x1	7	14	
Motorshaft	x1	0.4	0.4	C45 Steel
Bevelgear z=20	x1	3	3	C45 Steel
Bevelgear z=40	x1	9.6	9.6	C45 Steel
Gearshaft Press-fitted	x1	0.3	0.3	C45 Steel
Gearshaft bolted	x1	0.7	0.7	C45 Steel
Shaft Joint	x2	4.1	8.2	C45 Steel
Wheelshaft	x2	0.7	1.4	C45 Steel
Wheel	x2	1.7	3.4	Aluminum 6061
Motorbracket	x1			Aluminum 6061
Motorshaft-bracket and flangebearing	x1			Aluminum 6061
Bearinghouse	x2			Aluminum 6061
Bearingbracket	x2			Aluminum 6061

Table 3.2: Mass and Materials

FEM Results

The result of simulating the motorshaft gives a maximum stress of 120.1 MN/m^2 and thus a safety factor of 5.165 and is therefore stable enough for its area of application.

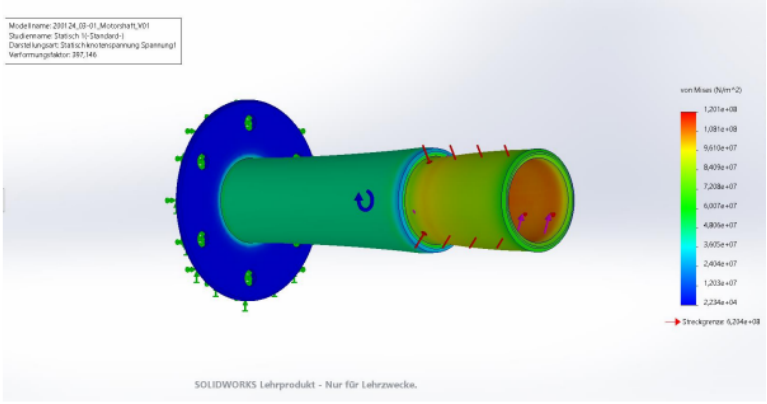

Figure 3.22: Finite Element Method (FEM) simulation results for the Motor shaft

The result of simulating the pressfitted gearshaft gives a maximum stress of $286.1\,\mathrm{MN/m^2}$ and thus a safety factor of 2.027 and is therefore stable enough for its area of application.

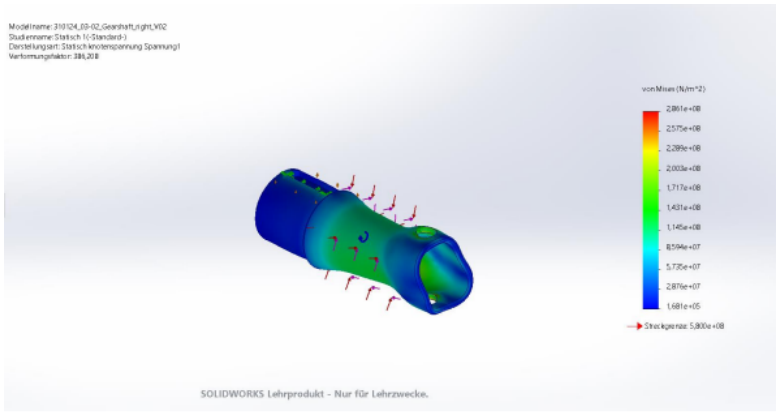

Figure 3.23: Finite Element Method (FEM) simulation results for the pressfitted Gearshaft

The result of simulating the bolted gearshaft gives a maximum stress of $288.1\,\mathrm{MN/m^2}$ and thus a safety factor of 2.013 and is therefore stable enough for its area of application.

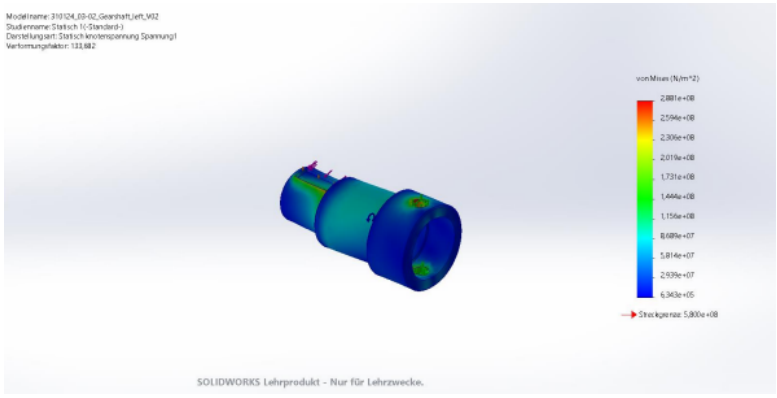

Figure 3.24: Finite Element Method (FEM) simulation results for the bolted Gearshaft

The result of simulating the wheelshaft gives a maximum stress of $284\,\mathrm{MN/m^2}$ and thus a safety factor of 2.042 and is therefore stable enough for its area of application. As this part is identical on both sides of the pod and has to withstand the same forces, we are only showing a single simulation here.

The result of simulating the wheel gives a maximum stress of $19.89\,\mathrm{MN/m^2}$ and while we manufacture this of a Aluminum 6061 compuond, a safety factor of 2.772 and is therefore stable enough

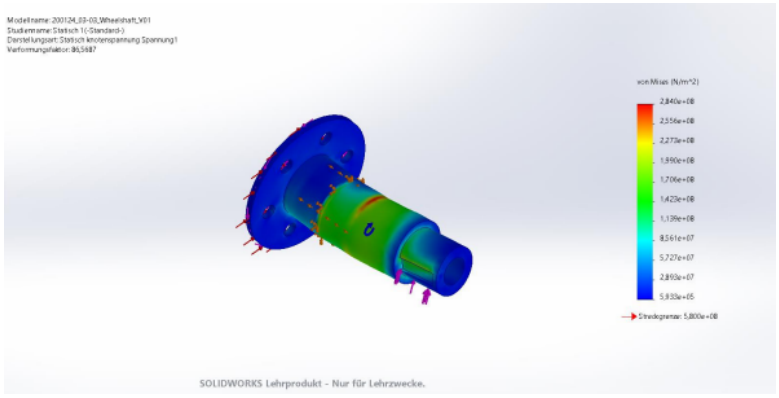

Figure 3.25: Finite Element Method (FEM) simulation results for the wheelshaft

for its area of application. As this part is identical on both sides of the pod and has to withstand the same forces, we are only showing a single simulation here.

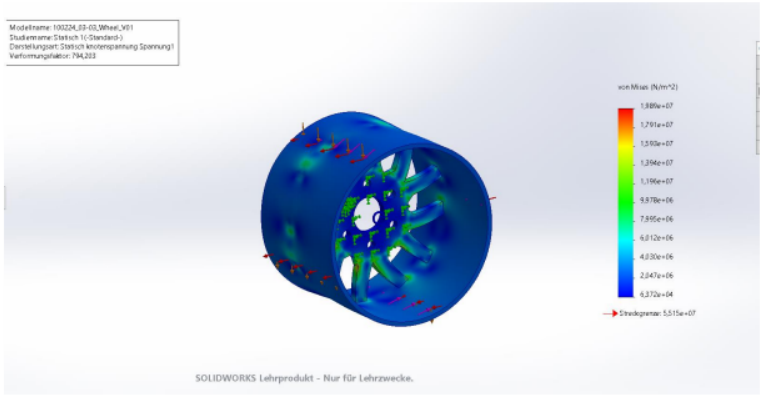

Figure 3.26: Finite Element Method (FEM) simulation results for the wheels

The result of simulating the motorbracket gives a maximum stress of XX N/m^2 and thus a safety factor of XX and is therefore stable enough for its area of application. As this part is identical on both sides of the pod and has to withstand the same forces, we are only showing a single simulation here.

The result of simulating the motorshaftbracket gives a maximum stress of XX N/m^2 and thus a safety factor of XX and is therefore stable enough for its area of application. As this part is identical on both sides of the pod and has to withstand the same forces, we are only showing a single simulation here.

The result of simulating the bearinghouse gives a maximum stress of XX N/m^2 and thus a safety factor of XX and is therefore stable enough for its area of application. As this part is identical on both sides of the pod and has to withstand the same forces, we are only showing a single simulation here. As this part is identical on both sides of the pod and has to withstand the same forces, we are only showing a single simulation here.

The result of simulating the bearingbracket gives a maximum stress of XX N/m^2 and thus a safety factor of XX and is therefore stable enough for its area of application. As this part is identical on both sides of the pod and has to withstand the same forces, we are only showing a single simulation here. As this part is identical on both sides of the pod and has to withstand the same forces, we are only showing a single simulation here.

Mesh and Boundary Conditions

For meshing and specify all required parameters for a successful simulation, we used the standardsettings of Solidworks.

3.2.3 Manufacturing Process

Component	Number	Required procedures
Motorshaft	x1	latheturning, milling
Gearshaft Pressfitted	x1	latheturning, milling, hydraulic pressing
Gearshaft bolted	x1	latheturning, milling
Wheelshaft	x2	latheturning, milling
Wheel	x2	latheturning, milling
Motorbracket	x1	lasercutting
Wheelshaftbracket	x1	lasercutting
Bearinghouse	x2	lasercutting
Bearingbracket	x2	lasercutting, welding

Table 3.3: Components and Manufacturing Details

3.2.4 Integration process

Assembling

Describe how the parts will be assembled, including integration into subordinate structures/systems if applicable.

Assembly interaction

If applicable, describe how the assembly interacts with other assemblies.

3.2.5 Safety considerations

(a) Discuss the safety factor applied to structural elements.
(b) If applicable, discuss the safety factor applied to the demagnetization of permanent mag- nets.
(c) If applicable, discuss high voltage safety considerations for the motor.
(d) Discuss worst-case scenarios (e.g., worst-case braking deceleration) and what you plan to do to avoid or contain them.

3.2.6 FMEA

WILL BE DONE BY PM

Expected Outcomes

Detail the anticipated results from the testing and validation processes.

Risk Mitigation

Discuss the potential risks associated with the system and how they will be mitigated.

Impact Resistance Detail a contingency plan in case the system does not perform as expected.

3.2.7 Testing

Provide a test plan including setup, procedure, and expected outcomes. Outline which factors are critical to success and how they will be validated.

3.2.8 Full-scale adaptation

- Funktioniert wie herkömmliche Eisenbahn - Für die Beschleunigung im Full scale möglich - Sobald der Pod mit levitation anfängt, werden die Reifen angehoben, und das derzeitige propulsion system abgeschaltet

3.2.9 References

EMRAX 188 Technical Data Table

Type / Technical data	EMRAX 188 High Voltage			EMRAX 188 Medium Voltage			EMRAX 188 Low Voltage		
Air cooled = AC Liquid cooled = LC Combined cooled = Air + Liquid cooled = CC	AC	LC	CC	AC	LC	CC	AC	LC	CC
Ingress protection	IP21	IP65	IP21	IP21	IP65	IP21	IP21	IP65	IP21
Cooling medium specification (Air Flow = AF; Inlet Water/glycol Flow = WF; Ambient Air = AA) If inlet WF temperature and/or AA temperature are lower, then continuous power is higher.	AF=20m/s; AA=25°C	WF=8l/min at 50°C; AA=25°C	WF=8l/min at 50°C; AA=25°C	AF=20m/s; AA=25°C	WF=8l/min at 50°C; AA=25°C	WF=8l/min at 50°C; AA=25°C	AF=20m/s; AA=25°C	WF=8l/min at 50°C; AA=25°C	WF=8l/min at 50°C; AA=25°C
Weight [kg]	6,8	7,0	7,0	6,8	7,0	7,0	6,8	7,0	7,0
Diameter ø / width [mm]	188 / 77								
Maximal battery voltage [Vdc] and full load/no load RPM	400 Vdc (6400/7600 RPM)			270 Vdc (6750/7830 RPM)			100 Vdc (7000/7800 RPM)		
Peak motor power at max RPM (few min at cold start / few seconds at hot start) [kW]	**70**								
Continuous motor power (at 3000-6000 RPM) depends on the motor RPM [kW]	**15 - 28**	**15 - 30**	**17 - 35**	**15 - 28**	**15 - 30**	**17 - 35**	**15 - 28**	**15 - 30**	**17 - 35**
Maximal rotation speed [RPM]	**7000 (8500 peak for few seconds)**								
Maximal motor current (for 2 min if cooled as described in Manual) [Arms]	200			300			800		
Continuous motor current [Arms]	100			150			400		
Maximal peak motor torque [Nm]	**100**								
Continuous motor torque [Nm]	**50**								
Torque / motor current [Nm/1Aph rms]	0,60			0,39			0,15		
Maximal temperature of the copper windings in the stator and max. temperature of the magnets [°C]	120								
Motor efficiency [%]	92-98%								
Internal phase resistance at 25 °C [mΩ]	/			/			/		
Input phase wire cross-section [mm²]	10,2			15,2			38		
Wire connection	star								
Induction Ld/Lq [µH]	/			/			/		
Controller / motor signal	sine wave								
AC voltage between two phases [Vrms/1RPM]	0,0384			0,0252			0,00923		
Specific idle speed (no load RPM) [RPM/1Vdc]	19			29			78		
Specific load speed (depends on the controller settings) [RPM/1Vdc]	16 – 19			25 – 29			70 – 78		
Magnetic field weakening (for higher RPM at the same power and lower torque) [%]	up to 100								
Magnetic flux – axial [Vs]	/			/			/		
Temperature sensor in the motor	kty 81/210								
Number of pole pairs	10								
Rotor Inertia (mass dia=160mm, m=3,0kg) [kg*cm²]	/								
Bearings (front:back) - SKF/FAG	6204:6204 (for radial forces) or 6204:7204 (for axial-radial forces; for pull mode; focusing on very high axial load, e.g. for air propeller) or 6204:3204 (for axial-radial forces; for pull-push mode; »O« orientation, α=25°); other bearings are possible (exceptionally)								

Figure 3.27: Motor Specifications

3.3 Cooling System

3.3.1 Overview

Requirements and Constraints

The cooling system plays a pivotal role in keeping the motor, battery, and traction controller within safe temperature limits. Overheating can lead to reduced efficiency and potentially shorten the lifespan of these components. For instance, excessive heat could cause bearings to wear out faster, damage motor windings, and even demagnetize permanent magnets. Given the hyperloop's low-pressure environment, we must think beyond standard air cooling methods. Consequently, the exploration of alternative cooling techniques, such as liquid cooling, cooling with the Phase Changing Materials are becoming imperative for ensuring the system's reliability and efficiency.

Estimated Cost and Part List

The total estimated manufacturing cost for the cooling system is approximately 1200 Euros, considering the primary components outlined in the table. Despite its comprehensive functionality, the system maintains a relatively lightweight and compact profile, comprising only a select few components. This cost-effective design approach ensures efficient performance without compromising on reliability or functionality.

Table 3.4

Table 3.4: Components and Manufacturing Details

Component	Number	Mass [kg]	Size [mm]	Material	Manufacturing process	In-house/ Outsourced
Heat Exchanger	x1	1.1	100 x120 x100	Aluminum	LPBF Printing	in-house
Drain Valve	x1	0.02	M8	Aluminum	Latheturning	in-house
PCM	x1.75 [liters]	2	-	PCM	-	outsourced
Deionized Water	x3 [liters]	3	-	Water	-	outsourced
Coolant Pump	x1	1.2	-	-	-	outsourced
Filter	x1	0.1	-	-	-	outsourced
Coolant Temperature Sensor	x2	0.2	-	-	-	outsourced
Surface Temperature Sensor	x3	0.2	-	-	-	outsourced
Flow Meter	x1	0.1	-	-	-	outsourced
Pressure Sensor	x4	0.1	-	-	-	outsourced
Piping	x5 [meters]	0.9	10 x 16	-	-	outsourced
Piping	x2 [meters]	0.4	20 x 26	-	-	outsourced
Tank	x1	0.2	138 x 160	-	-	outsourced
Fittings	x15	-	-	-	-	outsourced

3.3.2 Objectives, Design process, and Cooling Requirements

Figure 3.28

Motor

The EMRAX motor is required to operate within a temperature range of -40□C to 120□C for both the copper windings and magnets. To safeguard against overload, a temperature sensor is integrated into the motor and must be linked to the controller. If the temperature surpasses the permissible limit, the controller adjusts the motor's current output to lower levels until the temperature stabilise

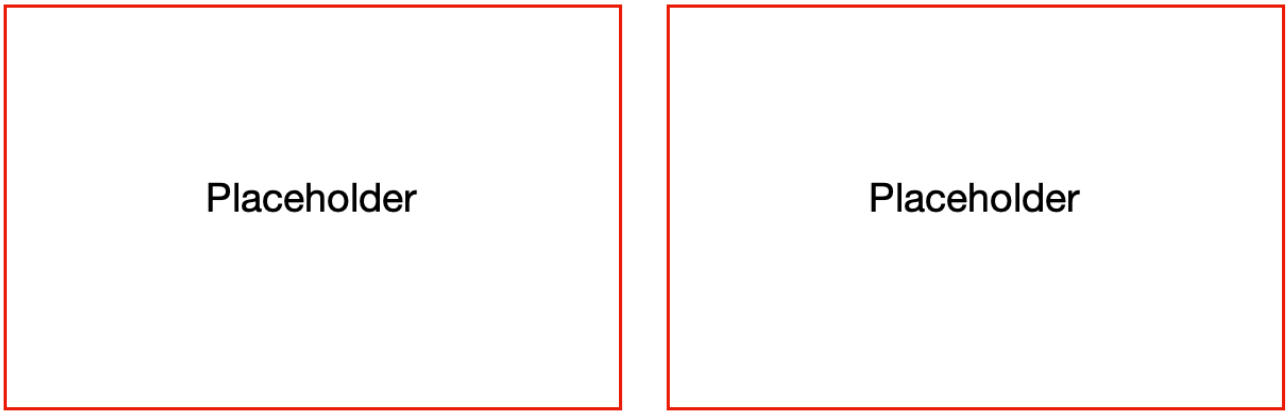

(a) Front view of the pod (b) Top view of the pod

Figure 3.28: Placement of the Cooling system

within the acceptable range, with a worst-case motor efficiency of 92%, approximately 4.8 kW of heat is generated during operation.

The manufacturer recommends a coolant flow rate of 6 to 8 litres per minute, with the coolant maintained at a maximum temperature of 50°C when entering the motor. Additionally, ambient air temperature surrounding the motor should ideally be 25°C or lower. [Ref - Product Spec Emrax Motor]

Traction Controller

According to the product specification, the maximum permissible temperature for the traction controller is 150°C. However, to guarantee peak performance and longevity, it's essential to maintain temperatures below 90°C. After assessing the operating current and internal resistance, the estimated heat generation was calculated to be 0.56 kW. Through heat transfer calculations from the power module baseplate, equipped with fins, to the coolant, a water flow rate of 0.7 litres per minute was determined necessary to sustain the traction controller's temperature at 90°C.This ensures optimal cooling performance and contributes to the longevity and efficiency of the entire cooling system.

Battery

The battery system within the hyperloop pod generates approximately 3.84 kW of heat during operation. This heat generation is primarily due to internal resistance within the battery cells as electrical energy is converted into usable power. To maintain safe and efficient operation, it is imperative to ensure that the temperature of the battery remains below 75°C.

When a battery operates at elevated temperatures, several detrimental effects may occur. High temperatures can accelerate the degradation of battery components, including the electrolyte and electrode materials, leading to reduced battery capacity and lifespan. Additionally, overheating increases the risk of thermal runaway, a phenomenon where the battery temperature rapidly increases, potentially resulting in fire or explosion.

Cooling Requirements and Strategies

To mitigate these risks and ensure the longevity and safety of the battery system, effective cooling strategies are essential. This includes implementing cooling systems, such as liquid cooling or cooling plates, to dissipate the heat generated by the battery during operation.

To ensure optimal cooling for all three vital components, the system necessitates a total coolant volume of 1 liters of de-ionised water. This calculation factors in the total heat generation (9.2 kW),

the duration of a single run at the European Hyperloop Week Competition (20 seconds), and a safety factor of 3 (total time 60 seconds). After 60 seconds of operation, the maximum temperature of the 3 liters of coolant reaches approximately 66.5□C, well below the specified temperature limits. Further analysis during testing phase will provide valuable insights into coolant temperature changes and component temperatures.

To enhance the cooling performance of the cooling System, a refined hardware architecture will be implemented. Temperature levels play a critical role in determining the durability and efficiency of the motor, battery, and traction controller within the hyperloop pod. Elevated temperatures can adversely affect various components, including bearings, motor windings, and permanent magnets, potentially leading to demagnetisation. Therefore, prioritising the enhancement of cooling systems is essential for achieving significant long-term cost savings and improved performance. Given the impracticality of air cooling in the low-pressure hyperloop tube environment, alternative approaches such as liquid cooling and the use of Phase changing materials must be explored.

Hardware Architecture for Enhanced Cooling

As illustrated in figure 3.32, cold water stored at room temperature (approximately 20-25□C) will undergo filtration and then be pumped into the water jackets of the motor, traction controller, and battery in a closed-loop configuration, with a flow rate ranging from 8 to 12 liters per minute. Continuous monitoring of the coolant, motor, traction controller, and battery temperatures will be conducted. Should the temperature of any component exceed the specified limit, the control system will promptly deactivate the pod's drive motor.

Given the absence of heat transfer with the atmosphere during operation, the coolant temperature will gradually increase. Consequently, it's imperative that the coolant within the system remains below the temperature limits of each component. Cooling down the coolant prior to the pod's subsequent operation will be necessary.s Pressure sensors have been strategically positioned at designated locations, as depicted in the diagram, to accurately gauge pressure drops across the water jackets during the testing phase. This data will be instrumental in fine-tuning the system's performance and ensuring optimal cooling efficiency.

3.3.3 Appearance and Integration

Coolant

Deionized water has been selected as the primary coolant for the system due to its low electrical conductivity. This choice is paramount in minimising the potential adverse effects of coolant leaks on the pod's electronic components. Although glycol is a common coolant choice in many cooling systems, it is not utilized in this particular system. This decision is attributed to the fact that the operating temperatures within the system consistently remain well above the freezing point of water, rendering glycol unnecessary.

Coolant Pump

During the testing phase, the Rheinmetall WUP 25 pump will serve as the primary pump for the cooling system. Although typically employed in the realm of combustion engines and vehicle climate control systems, the WUP 25 pump demonstrates versatility by effectively handling various cooling tasks, including cooling DC/DC converters, batteries, electric motors, and power electronics. Its compact design allows for installation in constrained spaces, and it offers a range of hydraulic and electrical interfaces to suit diverse applications. Equipped with a control and diagnostic pin, the WUP 25 pump facilitates speed control via a PWM input signal [Ref = Product Data Sheet WUP 25].

To ensure optimal performance, the pump will be mounted at a mid-level position within the cooling circuit. This strategic placement helps prevent the formation of air traps (if mounted at

the highest position) and minimizes the risk of debris accumulation within the pump (if mounted at the lowest position) [Ref = Product Data Sheet WUP 25]. However, due to the current uncertainty regarding the pressure drop in the system, it may be necessary to explore alternative pump options or implement a multi-stage pump system (in series) alongside the existing model. The exact pressure drop across the water jackets will be determined through rigorous testing

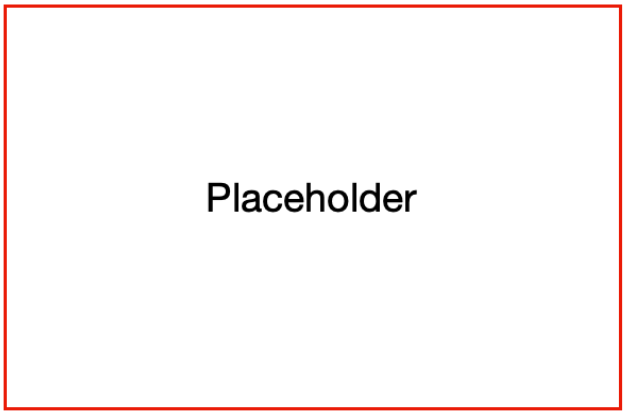

Figure 3.29: Coolant pump

Coolant Storage Tank

The cooling system is designed with consideration for the realistic scenario of the pod traveling through a low-pressure tube (near vacuum), limiting heat exchange with the atmosphere. The coolant in the circuit absorbs heat from the motor, battery, and traction controller, causing an increase in coolant temperature over time. The current design ensures sufficient coolant storage to keep all components well below the required maximum operating temperature.

For the hyperloop pod slated for participation in the European Hyperloop Week, a typical vehicle coolant tank with a capacity of 1 liter has been deemed adequate. This capacity aligns with the demands of the pod's cooling requirements, guaranteeing optimal performance throughout its operation.

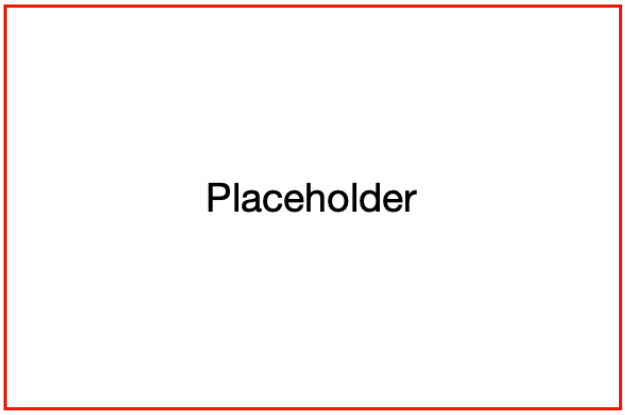

Figure 3.30: Coolant tank

Water Jackets

The water jacket for the motor will be provided by the motor manufacturer, ensuring compatibility and optimal performance. For the water jackets of the traction controller and battery, custom

fabrication will be undertaken based on the recommendations provided by their respective manufacturers. This approach guarantees that each component receives tailored cooling solutions to meet its specific requirements and operating conditions.

Piping

Two piping options are under consideration. i) CPVC pipes, chosen for their resistance to high temperatures, scaling, durability, low cost, and ease of installation. The specific piping route is yet to be finalized , but the total length is estimated to be around 6 meters. ii) The potential use of soft tubing is also being explored.

3.3.4 Heat Exchanger

Role and Benefits in the cooling System

In the context of the cooling system described for the hyperloop pod, a heat exchanger would play a crucial role in transferring heat between the coolant circulating within the closed-loop system and the surrounding environment. As the coolant circulates through the system, it absorbs heat from the motor, battery, and traction controller, thereby increasing in temperature. Since the hyperloop pod operates in a low-pressure tube with limited heat exchange with the atmosphere, the heat exchanger facilitates the dissipation of heat even in this constrained environment.

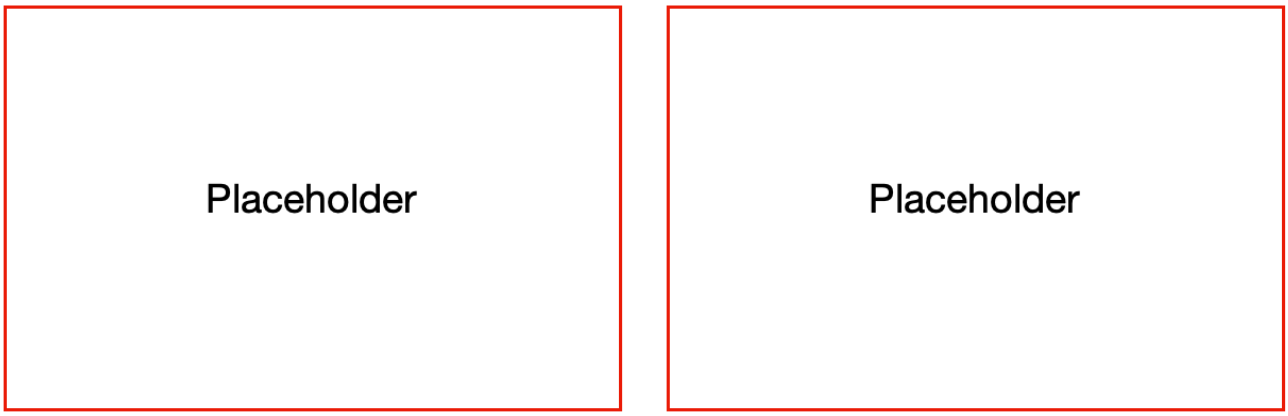

(a) Closed View (b) Open View

Figure 3.31: Gyroid Heat Exchanger

Use of Phase Change Materials (PCMs)

Introducing the heat exchanger utilizing phase change materials (PCMs) into the cooling system for the hyperloop pod would offer several advantages and could enhance its performance in specific scenarios, incorporating a heat exchanger with the use of phase changing material serves several important purposes:

- Enhanced Heat Absorption and Release: The PCM, such as stearic acid, can absorb and release a significant amount of heat during its phase transition from solid to liquid and vice versa. Integrating a heat exchanger with PCM allows for efficient absorption of excess heat generated by components like the motor, traction controller, and battery.
- Temperature Regulation: By absorbing excess heat from critical components, the heat exchanger helps regulate their temperatures within the specified operating ranges. This prevents overheating, which can lead to performance degradation or damage to components.

- Thermal Energy Storage: The PCM's ability to store thermal energy during its phase change enables the system to store heat when temperatures are within acceptable limits and release it when needed to maintain optimal operating conditions. This helps in managing transient heat loads and stabilizing temperatures over time.
- Reduced Coolant Temperature: By utilizing the PCM's heat absorption capacity, the heat exchanger can lower the temperature of the coolant circulating in the system. This ensures that the coolant remains within acceptable temperature limits, contributing to the overall effectiveness of the cooling system.
- Increased Efficiency: Integrating a heat exchanger with PCM can improve the overall efficiency of the cooling system by maximizing heat transfer capabilities and reducing the reliance on conventional cooling methods alone.
- Extended Operating Time: The thermal energy stored in the PCM can be utilized to extend the operating time of the system before coolant temperature rises beyond acceptable levels. This can be particularly beneficial during transient operating conditions or in the event of temporary power interruptions.

Overall, incorporating a heat exchanger with the use of phase changing material adds an additional layer of heat management capability to your cooling system, contributing to improved performance, efficiency, and reliability in the hyperloop pod environment.

Stearic Acid

Stearic acid stands out as a highly versatile phase change material (PCM) deployed across diverse applications. Its unique characteristic of transitioning from solid to liquid state at a precise temperature renders it exceptionally suitable for thermal energy storage purposes. Through this phase transition, stearic acid exhibits remarkable heat absorption and release capabilities, making it a valuable asset in scenarios demanding efficient temperature regulation and thermal energy management. Commonly found in applications ranging from building insulation to specialized temperature control systems, stearic acid's efficacy as a PCM underscores its widespread industrial utility.

Stearic Acid Stearic acid is a saturated fatty acid with the chemical formula $C_{18}H_{36}O_2$. It is a long-chain carboxylic acid, meaning it has 18 carbon atoms in its hydrocarbon chain and a carboxyl group (COOH) at one end. Here are some key properties and uses of stearic acid:

Physical Properties:

- Melting Point: Stearic acid is a solid at room temperature and has a melting point of around $69 - 70$ degrees Celsius ($156 - 158$ degrees Fahrenheit).
- Appearance: It is a white, waxy solid with a characteristic fatty odor.

Chemical Properties:

- Structure: Stearic acid has a straight-chain structure with 18 carbon atoms, making it a saturated fatty acid. Hydrophobic: Like other fatty acids, stearic acid is hydrophobic, meaning it repels water.

In summary, stearic acid is a versatile compound with various industrial applications, and its phase change properties make it useful in thermal energy storage applications as well.

3.3.5 Calculations and Simulations

WILL BE ADDED SOON (Dino)

3.3.6 Safety Measures

Given the close integration of the cooling system with the electronic systems, the primary risk is a coolant leak that could potentially damage electronic components. Preventive measures are outlined in the table below, and deionised water is chosen as the preferred coolant due to its low conductivity.

Potential Failure Modes and Risk Mitigation-

- Coolant Leaks
  - Effect of Failure: Damage Electronic components
  - Root Cause: Poor sealing at pipe joints
  - Risk Mitigation Strategy: Maintain the correct coolant level, avoid overfilling the tank, sealing pipes with hose clamps and use deionized water as a coolant.
- Temperature of Critical component rises above rated temperature
  - Effect of Failure: Damage Component
  - Root Cause: Insufficient cooling due to prolonged operation
  - Risk Mitigation Strategy: Implement a control system to halt the motor and by installing two temperature sensors if temperatures exceed prescribed limits for the motor, battery, or traction controller.
- Temperature of Critical component rises above rated temperature
  - Effect of Failure: Coolant Leaks
  - Root Cause: Insufficient cooling due to air traps or exceeding defined operation time
  - Risk Mitigation Strategy: Position of the system including heat exchanger is placed at the front of the pod, in order to purge air after refilling, and adhere to defined operation times.
- Blocks in piping
  - Effect of Failure: Insufficient cooling and damage to components
  - Root Cause: Foreign particles/debris
  - Risk Mitigation Strategy: Introduce filters in the piping system and conduct regular cleaning maintenance.

FMEA analysis

Failure Mode: Coolant Leaks

- Effects of Failure: Damage to Electronic components
- Severity: High
- Causes of Failure: Poor sealing at pipe joints
- Occurrence: Medium

- Current Controls: Regular inspection for leaks, pressure testing of the system
- Detection: Visual inspection, pressure sensors
- Risk Priority Number (RPN): Severity Occurrence Detection
- Recommended Actions: Improve seal quality, implement redundant sealing, increase inspection frequency
- Responsibility: Mechanical Team
- Actions Taken: Upgraded sealing materials, added secondary containment
- Revised RPN: After action taken

Failure Mode: Temperature of Critical Component Rises Above Rated Temperature (First Instance)

- Effects of Failure: Damage to Component
- Severity: High
- Causes of Failure: Insufficient cooling due to prolonged operation
- Occurrence: High
- Current Controls: Thermal cutoff switches, temperature monitoring
- Detection: Thermal sensors with automated system feedback
- Risk Priority Number (RPN): Severity Occurrence Detection
- Recommended Actions: Implement more efficient cooling mechanisms, revise operational protocols to prevent prolonged operation without cooling
- Responsibility: Electrical Team
- Actions Taken: Included additional cooling systems, adjusted operational limits
- Revised RPN: After action taken

Failure Mode: Temperature of Critical Component Rises Above Rated Temperature (Second Instance)

- Effects of Failure: Coolant Leaks
- Severity: High
- Causes of Failure: Insufficient cooling due to air traps or exceeding defined operation time
- Occurrence: Medium
- Current Controls: Coolant system design to avoid air traps, operational time limits
- Detection: Temperature and flow sensors
- Risk Priority Number (RPN): Severity Occurrence Detection
- Recommended Actions: Redesign of the coolant flow paths to eliminate air traps, strict adherence to operational time limits
- Responsibility: Design Team

- Actions Taken: Coolant flow paths optimized, operational procedures updated
- Revised RPN: After action taken

Failure Mode: Blocks in Piping

- Effects of Failure: Insufficient cooling and damage to components
- Severity: Medium
- Causes of Failure: Foreign particles/debris
- Occurrence: Low
- Current Controls: Filtration systems, preventive maintenance schedules
- Detection: Flow rate monitoring, pressure differential sensors
- Risk Priority Number (RPN): Severity Occurrence Detection
- Recommended Actions: Improve filtration system, implement more rigorous maintenance and cleaning schedules
- Responsibility: Maintenance Team
- Actions Taken: Upgraded filters, more frequent cleaning
- Revised RPN: After action taken

References

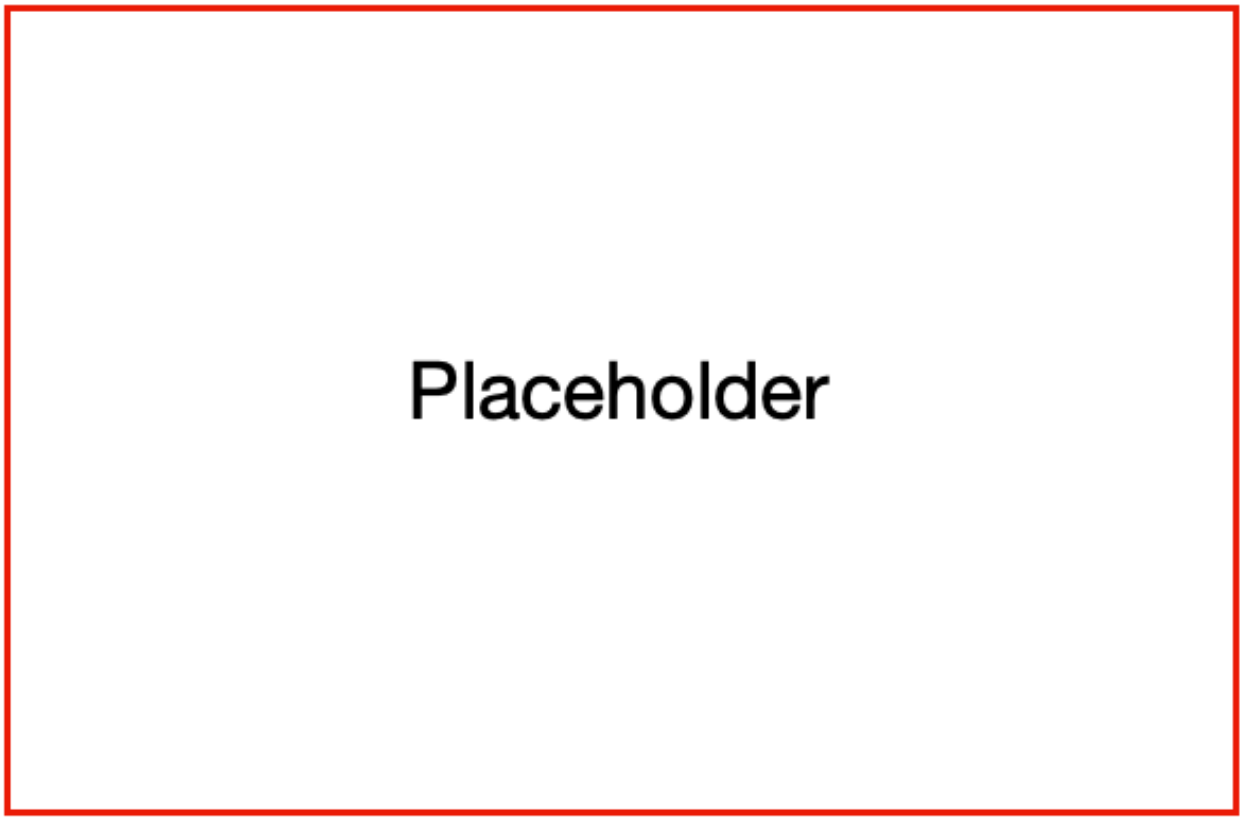

Figure 3.32: Flowchart of the system

3.4 Eddy Current Braking

Due to unexpected changes in the team, we decided to halt the development of an eddy current brake, which would have served as an addition to our friction brake, which will conform to the standards of the competition after the redesign that is shown in the respective section.

Electrical Systems

Take a short look at the whole text before starting to write your part.

4.1 Introduction

4.1.1 (b) List of all discrete electrical subsystems.

We are implementing the following subsystems:

- LV Battery
- HV Power Supply, including
  - Battery Management System
  - Insulation Monitoring Device
- Traction Inverter
- Propulsion Motor
- Sense and Control System

4.1.2 (a) Brief overview with the main points of the HV and LV systems.

Our electrical system provides the electrical power for the propulsion and control systems. We have a low voltage circuit at 24V (for control systems) and a high voltage level circuit at 444V (for the traction system). The low voltage circuit activates and controls the high voltage power supply through the Battery Management System and is hence designed for reliability.
The high voltage circuit is designed for safety, being potentially lethal, and power, in order to maximize the use of the motor. An OEM Insulation Monitoring Device checks for the (lack of) resistance between chassis and the HV power line in case of short circuits.
The traction inverter uses the electric power of the high voltage battery to power the motor, converting DC power into AC phases. We use an OEM device that is used in automotive purposes.
The motor is a motorsports motor from Emrax. Even though it belongs to the traction system, we will document it in the electrical section, as the development team of the originally planned inhouse-built inverter took over the duty of the electrical part of the motor system, too.
The Sense and Control System is not part of the EHW definition of the electrical systems. Since we have to provide a documentation nonetheless and the team designing the electrical subsystem also designed the Sense and Control system, we decided to include it as a part of the electrical subsystem documentation. It controls the brakes, the thermal pump, the telemetry line and the telemetry unit, as well as additional physical sensors.

Our general design of this season is inspired by conventional modes of transportation, as we have not had the capacity to start developing a levitation system by this season Thus, we focussed on an electrical system that drives our friction-based motor with excelling acceleration, which is a problem that railway systems frequently face.

In between design and production phase, we received a sponsorship of Leadrive, a local startup for research on automotive power electronics. Furthermore, the institute for electrical systems (ISEA) of our home university offered us assistance in the production of battery cells. Therefore, our workload was eased, which turned out to be favorable because of our lack of team members in the electrical field. This has been a crucial constraint in the design and planning process of the electrical department since the last season. Only shortly before submitting the ITD, we were able to make an estimation of realistic goals for the new team.

This year, we would like to set the path for magnetic levitation in the future, relying on an active system inside the vehicles. This was taken into consideration when designing the power dimensions, keeping plenty of overhead for the future, which aligns with our goal of sustainability. By having reusable modules, the design process of the upcoming years will be simplified.

We collaborate with the following institutions for support in the electrical department (including S&C):

- Altium: Sponsored Licenses of PCB design software
- Festo: Sponsored mechanical components and sensors for pneumatic systems.
- Mouser Electronics: Sponsored certain electronics.
- Würth Elektronik: Sponsored certain electronics.
- Leadrive: Sponsored traction inverter
- Vector Informatik: Sponsored CANoe Suite, including technical training for CAN networks.
- Bender: Sponsored Insulation Monitoring Device.
- ISEA: Assembling our battery pack.

4.1.3 (c) Wiring diagram of the HV system.

To Sourajit.

4.2 LV Battery

4.2.1 Overview

(a) Explain the main requirements and constraints that drive the design.
Strict EHW rules
reliability
reusability
lightweight
power of pump, valves etc.

Our Low Voltage system drives all electrical and digital control systems of the Fermion. As stated previously, reliability is crucial in this case. A failure of any component may lead to the shutdown of critical systems, such as the battery management system. Furthermore, an overvoltage may potentially damage these systems, causing safety hazards. We had the option between building a LV battery pack from spare LiPo cells we ordered for the HV battery pack, and using automotive-grade ventilated lead-acid batteries. After considering the safety problems of

LiPo cells and the efforts of either building a second (smaller) LV BMS or taking the risk of having a singular point of failure by controlling both systems with the same BMS, powering the BMS with the cells it controls, we went for the approach with lead-acid batteries, that is widely used in automotive systems. It is regarded as more reliable and robust compared to the Lithium-Ion pendants that we use for the High Voltage System.

Power requirements

We consider the power consumption of all components in the low voltage power line for the power requirements:

(Moussa: Bitte finde die einzelnen Daten heraus. Pumpe ist Pierburg CW150A. Valve ist bei den brakes controllern. Raspberry Pi und Microcontroller passen.)

- Solenoid Valves: Assuming 4 valves à 5 Watts = 20 Watts
- Thermal Pump: Given the thermal pump specifications (12V, 9A), the power consumption is $12\,\text{V} \times 9\,\text{A} = 108\,\text{W}$ max.
- Raspberry Pi 4:
- Total power for 1 Raspberry Pi 4: $10\,\text{W}$.
- Microcontrollers (TIC2000 F280039C):
  - Microcontroller power consumption can vary. Assuming around 2 Watts for each microcontroller.
  - Total power for 3 microcontrollers: $3 * 2\text{W} = 6\,\text{W}$.
- BMS (Orion BMS 2 for 120 Cells):
  - Power consumption can vary based on the specific BMS model. Assuming around 10 Watts.
- Leadrive Inverter: Power consumption of the inverter can vary. Assuming around 50 Watts for this calculation.
- Network transceiver: We use the Rocket M2, which consumes up to 6 Watt of energy.

Now, summing up all the power requirements:

$$20\,\text{W} + 108\,\text{W} + 5\,\text{W} + 6\,\text{W} + 10\,\text{W} + 50\,\text{W} = 210\,\text{W}$$

So, the estimated power requirement for the system, considering these components, is approximately 210 Watts, or roughly 8.5 A at 24 V.
Using the discharge chart of the data sheet of the LV Battery (at Moussa: Bitte Bild von Discharge Time - Discharge Current einfügen), it is evident that even at full power (9A - including some headroom for losses), we can run our low voltage system for 20 minutes. During the competition, we can rule out that we will use that much power over the whole 20 minutes. If we assume that the thermal system is activated while the HV system is at work, and that this duration takes 2 minutes maximum (the actual run will be much less - max. 20 seconds), and we assume only a usage of 100 W for the rest of the time, we can use the LV battery for well over 20 minutes. In conclusion, the capacity of 9Ah is a trade-off between the mass and the available runtime of the system.

Battery Type	Lead-Acid(integrated)
Capacity[Ah]	9
Nominal Voltage[V]	12
Cell configuration	2s
Max. discharge [A]	10
Weight per cell [Kg]	2,7
Dimensions per cell (L x W x H)[mm]	151 x 65 x 94

Table 4.1: LV battery cell characteristics

Battery Type	Lead-Acid(integrated)
Capacity[Ah]	9
Nominal Voltage[V]	24
Cell configuration	2s
Max. discharge [A]	10
Weight [Kg]	5.5
Dimensions (L x W x H)[mm]	151 x 65 x 94

Table 4.2: LV battery pack characteristics

4.2.2 Electrical and mechanical design process

(a) Present Schematics or logic diagrams of the boards.

(b) Present temperature simulations for vacuum conditions.

For our heat simulations, we used the software of ANSYS. By vacuum conditions, we assumed the lack of gas flow, which eliminates the cooling heat flow from winds. The simulation tool solves the heat transfer equation $\frac{\partial T}{\partial t} = \alpha \left(\frac{\partial^2 T}{\partial x^2} + \frac{\partial^2 T}{\partial y^2} + \frac{\partial^2 T}{\partial z^2} \right)$ by discretizing through Finite-Element-Methods.

4.2.3 Electrical system characteristics

4.2.4 Interface with other system

Briefly reference the communication protocols or control mechanisms of the boards, which should be explained in the respective Sense and Control subsection.

All the electric subsystems are located within the pod.
It powers the entire sensing, control and telemetry system. The LV battery itself does not communicate. Its sensor data is processed by the thermal control board. When the voltage drops below a certain threshold, the complete system shuts down.

4.2.5 Final system description

The two lead-acid batteries, chained in series, provide a nominal voltage of 24V (12V each). When fully charged, the voltage can increase to up to 26V. The lead acid batteries have the problem of voltage drops while discharging. Hence, we monitor the voltage while using the LV battery system.

The 24 V power source gets transferred down to 12V (for the Thermal Pump) and 5V for the micro-controllers by buck converters, and drives the valves and several sensors at 24V simultaneously. It is being monitored by NTC thermistors for overheating, and by the thermal system for undervoltage.
After reaching out to the EHW technical committee, we were able to clarify that a BMS, used by Lithium-Ion batteries, is not required for lead-acid batteries due to the inherently different chemical structure which makes over- and undercharging much less critical.

For charging, we are using a battery charger specified for 12V and 24V lead acid cells from Würth 0510955908. The charging of lead-acid batteries in series is unproblematic, given that we regularly test for drifts and manually balance the cells.

4.2.6 Manufacturing process

As the cells come in hard-shell covers already, the manufacturing process is not very complicated. We will 3D-print a casing.

4.2.7 Testing

We will test whether the lead acid cells and the thermistors are accurate to their datasheet.

4.3 High Voltage Power Supply

4.3.1 Overview

(a) Explain the main requirements and constraints that drive the design.

4.3.2 Electrical and mechanical design process

(a) Present Schematics or logic diagrams of the boards.

(b) Present temperature simulations for vacuum conditions.

For our heat simulations, we used the software of ANSYS. By vacuum conditions, we assumed the lack of gas flow, which eliminates the cooling heat flow from winds. The simulation tool solves the heat transfer equation $\frac{\partial T}{\partial t} = \alpha \left(\frac{\partial^2 T}{\partial x^2} + \frac{\partial^2 T}{\partial y^2} + \frac{\partial^2 T}{\partial z^2} \right)$ by discretizing through Finite-Element-Methods.

4.3.3 Description of subsystem control

From | To	LV Battery	HV Battery	BMS	Traction Inverter	Motor	Cooling System
LV Battery	-	-	Powers	Powers control system	-	Powers pump and control system
HV Battery	-	-	Connects to	Provides power	-	-
BMS	-	-	Controls	-	-	-
Traction Inverter	-	-	-	-	Propels	X
Motor	-	-	-	-	-	-
Cooling System	-	-	-	Cooling	Cooling	Cooling (implicitly)

Table 4.3: Physical connection matrix

From \ To	LV Battery	HV Battery	BMS	Traction Inverter	Motor	Cooling System	Brakes Controller	Telemetry Unit
LV Battery	-	-	-	-	-	-	-	-
HV Battery	-	-	Discharge rate, voltage level	-	-	-	-	-
BMS	controls	controls	-	-	-	-	-	sends data
Traction Inverter	-	-	-	-	-	-	-	sends data
Motor	-	-	-	-	-	-	-	-
Cooling System	-	-	-	-	-	-	-	sends data
Brakes Controller	-	-	-	-	-	-	-	sends data
Telemetry Unit	-	-	updates limits	sends commands	-	sends target rates	sends commands	-

Table 4.4: Data connection matrix

(a) Briefly reference the control systems of the boards, which should be explained in the levitation or propulsion subsection respectively.

We configure the BMS prior to the competition.

4.3.4 Electrical system characteristics

4.3.5 Interface with other system

(a) Briefly reference the communication protocols or control mechanisms of the boards, which should be explained in the respective Sense and Control subsection.
All the electric subsystems are located within the pod.

The phsyical connection matrix is as following:
The data connection matrix is as following. All communication between boards are via CAN, if not specified otherwise:

4.3.6 Final system description

Battery Cells

High Voltage Network:

Our high voltage battery will make use of lithium-ion polymer technology. We use 120 pouch-format cells from Shenzhen GrePow Battery Co. Ltd rated at 45C maximum discharge that we plan to connect in series. The finished package (main battery pack) will be assembled by the team. We are going to connect the 120 cells connected in series and that will have 1 parallel line. This will roughly have 504 Volt at max (using $120 * 4.2V = 504V$) which provides sufficient electricity to power the motor. The battery pack will provide up to 350 Amps of DC current available to the inverter. However, neither the inverter nor the motor is not rated for such high currents nominally. Therefore, the maximum output current of the HV Battery will be rated at 200 A maximum (peak) and 100 A continuous.

We will stack 30 cells in series per pack and then stack 4 of them to get the full battery pack. No we won't.

BMS

Our battery management system

The Orion BMS 2, connected to the HV battery, protects it and improves its life, efficiency. Operational Mechanics

The Orion BMS 2 facilitates real-time monitoring and management of each cell within the HV battery pack, which consists of 120 lithium-ion polymer cells arranged in a series configuration to achieve a nominal voltage of 504V. This arrangement necessitates precise control and monitoring to prevent overcharging, deep discharging, and to ensure balanced cell voltages, all of which are within the Orion BMS 2's capabilities.

1. Cell Voltage Monitoring and Balancing: The BMS continuously monitors the voltage of each cell, ensuring that all cells operate within their safe voltage range. Cell balancing is performed to equalize the charge across all cells, thereby enhancing the battery pack's overall efficiency and lifespan.
2. Temperature Monitoring: Given the high energy density of the HV battery pack, thermal management is paramount. The Orion BMS 2 monitors the temperature of individual cells and the battery pack as a whole, activating cooling measures when necessary and preventing operation under extreme temperatures that could damage the battery or compromise safety. The Orion BMS 2 itself tracks the temperature of 8 individual cells. 28 other cells are measured by the Thermal Controller.
3. State of Charge (SoC) and State of Health (SoH) Estimation: SoC and SoH estimations are important for optimal battery utilization and health maintenance. The Orion BMS 2 employs advanced algorithms to provide these estimates, ensuring that the battery's capacity is used efficiently.

The integration of the Orion BMS 2 encompasses several safety mechanisms designed to protect the battery pack, the hyperloop pod, and its occupants:

1. Overcurrent and Short Circuit Protection: By monitoring the current flowing in and out of the battery pack, the Orion BMS 2 can detect overcurrent conditions and short circuits, initiating immediate shutdown procedures to prevent damage and ensure safety.
2. High and Low Voltage Protection: The BMS prevents the battery from exceeding its maximum voltage during charging and dropping below its minimum voltage during discharge, thereby avoiding scenarios that could lead to reduced battery life or safety hazards.
3. Thermal Runaway Prevention: Through its temperature monitoring capabilities, the Orion BMS 2 can detect the onset of thermal runaway—a dangerous condition where one cell's failure can lead to a cascading failure of adjacent cells—and take corrective actions to isolate the problem and mitigate potential damage.

Efficiency Enhancements

By optimizing the operational parameters of the HV battery pack, the Orion BMS 2 contributes significantly to the efficiency and performance of the hyperloop prototype:

1. Energy Optimization: By ensuring that all cells are balanced and operate within their optimal voltage and temperature ranges, the BMS maximizes the energy extracted from the battery pack, contributing to the hyperloop's range and speed capabilities.
2. Lifecycle Extension: Through diligent monitoring and management, the Orion BMS 2 extends the useful life of the HV battery pack, reducing the environmental impact and operational costs associated with battery replacement.
3. Predictive Maintenance: By providing detailed data on the SoC and SoH, the Orion BMS 2 enables predictive maintenance, allowing for timely interventions that prevent unscheduled downtimes and extend the battery's lifespan.

Conclusion

The integration of the Orion BMS 2 with the HV battery pack in our hyperloop prototype represents a critical step towards ensuring the system's safety, efficiency, and reliability. Through its comprehensive monitoring and management capabilities, the Orion BMS 2 ensures that the HV battery pack operates within its optimal parameters, significantly contributing to the prototype's overall performance and safety profile. As we progress towards the final stages of the FDD, the detailed exploration of the Orion BMS 2's functionalities underscores our commitment to leveraging advanced technologies for the enhancement of hyperloop transportation systems.

Insulation Monitoring Device

The Insulation Monitoring Device that is mandatory for EHW participants, as well as Formula Students teams, is not built inhouse, after receiving the respective advice from the EHW technical jury. By reaching out to Bender, we received their device through their Formula Students policy. It is configured for ...

4.3.7 Manufacturing process

Our PCB Design

PCBs

Prototyping: Prototype PCBs are fabricated in the FabLab associated with our university. The FabLab provides access to PCB manufacturing equipment and materials, enabling the rapid production of prototypes for initial testing and design validation. Once the PCBs are fabricated, they are assembled manually by our team members. Bigger PCBs are assembled in the facilities of the FabLab with the manual Pick and Place Machine and a reflow oven.

Production: We ordered our final PCBs from JLCPCB, a leading PCB manufacturing service. In addition to JLCPCB, we also collaborate with Würth Elektronik who produce PCBs in Germany, aligning with our goal of sustainability.

Batteries

The production of the low voltage battery pack is rather easy. We will use a 3d printer to print the casing We produced the battery packs in cooperation with the ISEA (Institute for Power Electronics and Electrical Drives) at RWTH, whose experience helped us to assemble and design the parts more efficienciently and more safely, as we had a considerable high voltage system. The casing will consist of polycarbonate. Polycarbonate is a material that is durable , lightweight, and impact resistant. The problems with material degradation through UV emissions does not impact us substantially, as we cover the battery pack inside the shell for most of the time. We will have safety measures preventing too much exposure to UV radiation. Also, the degradation is mainly of cosmetic nature (https://link.springer.com/article/10.1007/s11668-020-01002-9) .

4.3.8 Testing

We started testing software.

4.4 Power Electronics

4.4.1 Overview

(a) Explain the main requirements and constraints that drive the design.

Our general design of this season is inspired by conventional modes of transportation, as we have not had the capacity to start developing a levitation system by this season Thus, we focussed on an electrical system that drives our friction-based motor with excelling acceleration, which is a problem that railway systems frequently face.

In between design and production phase, we received a sponsorship of Leadrive, a local startup for research on automotive power electronics. Therefore, our workload was eased, which turned out to be favorable because of our lack of team members in the electrical field. This has been a crucial constraint in the design and planning process of the electrical department since the last season. Only shortly before submitting the ITD, we were able to make an estimation of realistic goals for the new team.

This year, we would like to set the path for magnetic levitation in the future, relying on an active system inside the vehicles. This was taken into consideration when designing the power dimensions, keeping plenty of overhead for the future, which aligns with our goal of sustainability. By having reusable modules, the design process of the upcoming years will be simplified.

4.4.2 Electrical and mechanical design process

Our initial goal was to design our own traction inverter system, both the control and power stages. After receiving the sponsorship with Leadrive, who also sponsors another student team in Aachen that we collaborate closely with, we decide to put our own, limited sources to other projects temporarily.
This means that we have a automotive inverter, with slightly overdimensioned specifications, to work with. We do have...
The DC link capacitor of the inverter ...
The precharge circuit was based on an economic decision. Our pod is not made for a commercial purpose. Thus, fast pre-/discharge times are not highly prioritized. We designed with several different precharge resistors at levels from 50 Ohm to 10 kOhm, and simulated them. The results showed that the low-resistance circuits need very high-power components, which will dissipate a lot of heat and be a potential safety danger. However, we wanted to keep the charging times within reasonable times (<5 seconds).
We simulated a test case with charging the capacitor to a stage where 99.5 □ is charged. Thus, the current flow when the main power line is switched on is well under 100A, which is the continuous rating of our system.
Finally, we chose a resistor with a lot of headroom: We used 3k resistor with a 50 Watt maximum rating.
This gives us the following specifications of our precharge circuit:

- Time Constant (τ):

$$\tau = R \times C = 3000\,\Omega \times 0.24 \times 10^{-3}\,\text{F} = 0.72\,\text{s}$$

- □□Voltage across the capacitor at $t = 5$ seconds□□:

$$V(5) = 500 \times \left(1 - e^{-\frac{5}{0.72}}\right) = 499.52V$$

- □□Rate of Charge at $t = 5$ seconds□□:

$$\left.\frac{dQ}{dt}\right|_{t=5} = C \times \left.\frac{dV(t)}{dt}\right|_{t=5} = 0.24 \times 10^{-3}\,\text{F} \times \frac{500}{0.72} \times e^{-\frac{5}{0.72}}$$

Now, we'll compute the numerical value for $\frac{dQ}{dt}$ at $t = 5$ seconds:

$$\left.\frac{dQ}{dt}\right|_{t=5} = 0.24 \times 10^{-3} \times \frac{500}{0.72} \times e^{-\frac{5}{0.72}} \approx 0.24 \times 10^{-3} \times 694.44 \times e^{-6.94}$$

$$\left.\frac{dQ}{dt}\right|_{t=5} \approx 0.16176\,\text{mA}$$

So, the rate of charge after 5 seconds is approximately 0.16176 mA. The power when switching to the main circuit is, thus, $500V * 0.16176mA = 0.081W$.
We can accept this. Furthermore, our simulations show that the maximum power will not exceed 22 W, whilst the main peak (>5W) lasts less than 2 seconds. The heat

(a) Present Schematics or logic diagrams of the boards.

(b) Present temperature simulations for vacuum conditions.

For our heat simulations, we used the software of ANSYS. By vacuum conditions, we assumed the lack of gas flow, which eliminates the cooling heat flow from winds. The simulation tool solves the heat transfer equation $\frac{\partial T}{\partial t} = \alpha\left(\frac{\partial^2 T}{\partial x^2} + \frac{\partial^2 T}{\partial y^2} + \frac{\partial^2 T}{\partial z^2}\right)$ by discretizing through Finite-Element-Methods.

4.4.3 Description of subsystem control

(a) Briefly reference the control systems of the boards, which should be explained in the levitation or propulsion subsection respectively.

We configure the BMS prior to the competition.

From | To	LV Battery	HV Battery	BMS	Traction Inverter	Motor	Cooling System
LV Battery	-	-	Powers	Powers control system	-	Powers pump and control system
HV Battery	-	-	Connects to	Provides power	-	-
BMS	-	-	Controls	-	-	-
Traction Inverter	-	-	-	-	Propels	X
Motor	-	-	-	-	-	-
Cooling System	-	-	-	Cooling	Cooling	Cooling (implicitly)

Table 4.6: Physical connection matrix

4.4.4 Electrical system characteristics

Parameter	MIN	NOM	MAX	Unit	Conditions
Ambient Temp. for Operation (T_{AMB})	-40	-	90	□C	-
Ambient Temp. for Storage (T_{STO})	-40	-	85	□C	-
Relative Humidity	0	-	95	□	-
Flow Rate of Coolant (V_{CLNT})	8	12	16	l/min	Derating @ $8 \sim 12$ l/min
Inlet Temp. of Coolant (T_{CLNT})	-40	-	85	□C	Derating @ $65 \sim 85$□C
Cooling Inlet Pressure (P_{INLET})	-	-	2.5	bar	-
Pressure Drop between Cooling Inlet and Outlet (P_{DROP})	-	0.25	-	bar	$T_{CLNT} = 65$□$C, V_{CLNT} = 12$ l/min
Input Voltage (V_{DC})	260	600	850	V	Full operation @ $450 - 800$V
Input Current (I_{DC})	-	200	-	A	Continuous
Peak Input Current (I_{DCPK})	-	300	-	A	For max t_{PK} duration
Output Voltage (V_{AC})	-	400	-	Vrms	-
Output Current (I_{AC})	-	-	200	Arms	Continuous
Peak Output Current (I_{ACPK})	-	-	300	Arms	For max t_{PK} duration
Output Power (S_{AC})	-	135	-	kVA	Continuous
Peak Output Power (S_{ACPK})	-	200	-	-	For max t_{PK} duration
Peak Duration (t_{PK})	-	-	60	s	-
Input Voltage for Control (V_{BAT})	6	-	36	V	Full functional @ $8 - 32$V (control board)
Max. Efficiency (η)	97	-	-	□	-
Torque Control Accuracy (ϵ_{TRQ})	-	-	3	□	Torque > 100Nm
	-	-	3	Nm	Torque < 100Nm
Torque Control Speed (t_{TRQ})	-	-	100	ms	-
Speed Control Accuracy (ϵ_{SPD})	-	-	30	rpm	-

Table 4.5: 800V Single Inverter Specifications

4.4.5 Interface with other system

(a) Briefly reference the communication protocols or control mechanisms of the boards, which should be explained in the respective Sense and Control subsection.
All the electric subsystems are located within the pod.

The phsyical connection matrix is as following:

The data connection matrix is as following. All communication between boards are via CAN, if not specified otherwise:

4.4.6 Final system description

Our inverter:

A precharge circuit:

From \ To	LV Battery	HV Battery	BMS	Traction Inverter	Motor	Cooling System	Brakes Controller	Telemetry Unit
LV Battery	-	-	-	-	-	-	-	-
HV Battery	-	-	Discharge rate, voltage level	-	-	-	-	-
BMS	controls	controls	-	-	-	-	-	sends data
Traction Inverter	-	-	-	-	-	-	-	sends data
Motor	-	-	-	-	-	-	-	-
Cooling System	-	-	-	-	-	-	-	sends data
Brakes Controller	-	-	-	-	-	-	-	sends data
Telemetry Unit	-	-	updates limits	sends commands	-	sends target rates	sends commands	-

Table 4.7: Data connection matrix

The MSD: We buy the devices from Amphenol

4.4.7 Manufacturing process

Our PCB Design

PCBs

Prototyping: Prototype PCBs are fabricated in the FabLab associated with our university. The FabLab provides access to PCB manufacturing equipment and materials, enabling the rapid production of prototypes for initial testing and design validation. Once the PCBs are fabricated, they are assembled manually by our team members.

Production: We ordered our final PCBs from JLCPCB, a leading PCB manufacturing service. In addition to JLCPCB, we also collaborate with Würth Elektronik who produce PCBs in Germany, aligning with our goal of sustainability.

Inverter

The inverter is a product from Leadrive used as an OEM product in automotive and mobility industry.

Support from Leadrive: The development of the inverter system is supported by Leadrive, a company specializing in advanced inverter technology. Their expertise significantly contributes to the optimization of our propulsion system. Collaboration with Formula Student Team of FH Aachen: Additionally, we collaborate with the Formula Student Team of FH Aachen, benefiting from their practical experience in electric vehicle design and inverter application. This partnership enriches our project with valuable insights into inverter integration and performance enhancement.

4.4.8 Testing

We started testing software.

4.5 Sensing and Control

4.5.1 Overview

Our S&C subsystem consists of a

- Control Boards:
  - Braking Controller
  - Thermal (Cooling) Controller
- Telemetry Device:

- CAN Bus
- Telemetry Transceiver
- Network Transceiver
- GUI/Logging system

In this section, the main components of the sensor network and software architecture shall be described, as well as their basic functionality. A special focus shall be made on how safety mechanisms are implemented in these systems. Extensive design descriptions are expected for, if applicable:

4.5.2 Control Boards

Introduction

1. Brief overview of all control boards (Brakes, Thermal)
2. Diagram with the connection of all boards with NAP and control station.
3. Brief description of communication protocols used.

Parts Lists

Example Thermal Parts list start: Parts List:

Amount	Name	Company (Serial Number)	Dimensions (mm
38	Additional Temperature Sensors (NTC, 10k Ohm)	Mouser	1000 x
1	Coolant Pump	Unknown	Unkno
1	MOSFET Bridge	Unknown	Unkno

Table 4.8: Description of Components

4.5.3 State Machine of the Vehicle

Our states are different for each component.

4.5.4 Code Architecture and Class Diagram

Brakes Controller

The software follow a simple state:

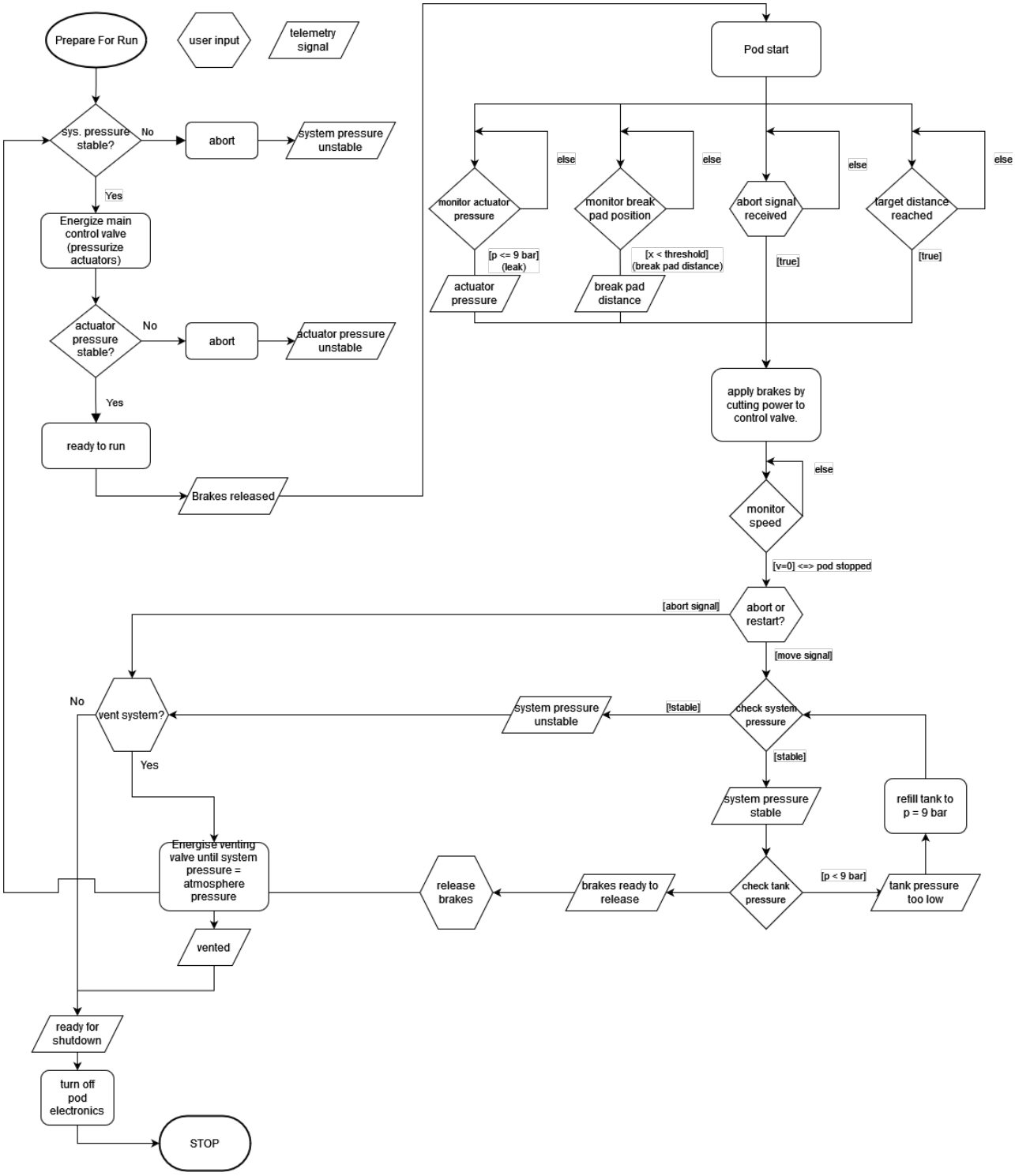

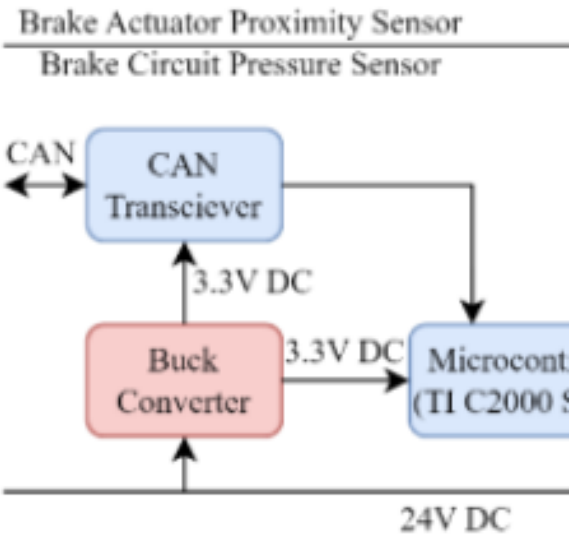

The implementation of the hardware architecture goes as follows:

Thermal Controller

it follows the following state diagram:
— INSERT STATE DIAGRAM —

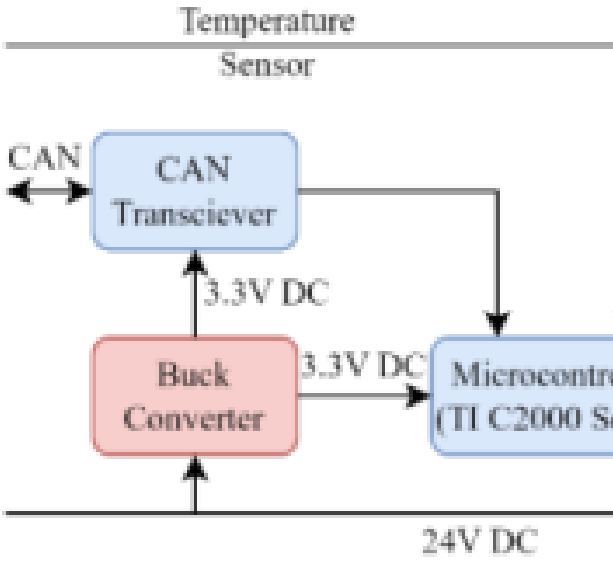

The following hardware architecture is to be implemented:

4.5.5 Control Boards/Units in the Vehicle

1. Brakes Controller Lacking. To be added.
2. Thermal Controller The Thermal Management Controller is responsible for cooling the Traction Components, i.e., Motor and Traction Controller. The actuator is the coolant pump which is controlled with the feedback of the temperature of coolant in the cooling loop. The Pump Speed is controlled via PWM to the MOSFET Bridge. The PWM duty cycle is simply calculated from a lookup table that is referenced to the temperature difference between target and actual temperatures. The only safety feature to be developed is to issue an emergency stop signal to HV Systems in the event the coolant temperature exceeds a critical temperature.

Parts List

Part	Manufacturer	Description
Raspberry Pi Zero 2 W	Raspberry	Microcontroller for telemetry
Raspberry Pi 4 B	Raspberry	Computer for telemetry
MC3479	Memsic	3-Axis Accelerometer
RS485 CAN HAT	Waveshare	CAN adapter for RPI4B

Table 4.9: Telemetry System Parts List

4.5.6 Integration with other systems

The friction brakes, the cooling pump and the motor are controlled through our system.

4.5.7 Graphical User Interface (GUI)

4.5.8 Telemetry Device

For communication and navigation, we use our telemetry system, that consists of a CAN bus, a CAN2WLAN transmitter and a VCU.

Introduction

1. Brief overview of Telemetry Components
2. Diagram with the connection of all boards with NAP and control station.
3. Explanation of the Signals Transmitted

Parts Lists

4.6 Additional considerations when writing the document for specific subsystems

Sources:

- https://link.springer.com/article/10.1007/s40789-022-00494-0 BMS System Reliability
-

Safety - 30 pages max

We have the following safety hazards:

- Pneumatic Braking Systems
- Heavy systems
- Cooling and Thermal Systems
- High voltage Batteries and protections

5.1 FDD.25 Technical Description for Compliance

5.2 FDD.26 Preliminary Risk Assessment for Demonstration

5.3 FDD.27 (FMEA)

5.3.1 Mechanical Systems FMEA

5.3.2 Electrical Systems FMEA

The following table details the Failure Mode and Effects Analysis for the Low Voltage Battery System used in the Tachyon Hyperloop prototype.

The following table details the Failure Mode and Effects Analysis for the High Voltage Battery System used in the Tachyon Hyperloop prototype.

Mitigation Strategies

Detailed strategies to address, reduce, or eliminate the risks associated with each identified failure mode, including design improvements, preventive maintenance, and enhanced monitoring systems.

Implementation and Follow-Up

Action plan for implementing the mitigation strategies, along with a process for ongoing monitoring and updating the FMEA based on operational experience and system modifications.

5.3.3 Traction Systems FMEA

5.3.4 Sense and Control Systems FMEA

5.3.5 Risk Mitigation Measures

Failure Mode	Potential Effects	Potential Causes	Current Controls	Severity	RPN
Cell Degradation	Reduced system performance, possible system shutdown, capacity	Aging, overuse, use at overtemperature	Monitoring of cell health, thermal control. Limit range of use to 20 □ to 80 □	Medium	TBD
Leakage	Short circuits, damage to other components	Mechanical stress, overcharging, manufacturing defects	Protective casing, visual inspection, BMS monitoring	Medium	TBD
Overcharging	Reduced battery life, risk of fire	Faulty charging system, operator error	Overcharge protection	High	TBD
Undercharging	reduced performance and life span	Faulty charging system, operator error	Monitoring system for charge level	Medium	TBD
Internal Short Circuit	Explosive fire hazard, complete system failure	Manufacturing defect, physical damage	Internal insulation	Very High	TBD

Table 5.1: FMEA for Low Voltage Battery System

5.4 FDD.28 Energy Storage Types and Components

5.5 FDD.29 Transport, Storage, and Lifting Requirements

5.5.1 FDD.26 Preliminary Risk Assessment for Transport and Lifting

5.5.2 Transport and Storage Logistics

Failure Mode	Potential Effects	Potential Causes	Current Controls	Severity	Occurrence	Detection	RPN
Thermal Runaway	Fire, explosion, damage to system	Overcharging, internal short, manufacturing defect	BMS, thermal monitoring and control	10	1	3	30
Overvoltage	Damage to electrical components, reduced battery life	Faulty BMS, charger malfunction	BMS, limit of charge	8	2	4	64
Undervoltage	Reduced performance, reduced health, system shutdown	High load, BMS failure	Low voltage detection, overdimensioning of battery power, automatic shutdown	6	3	5	90
Internal Short Circuit	Fire hazard, battery failure	Manufacturing defect, physical damage	Protective Device (Insulation Monitoring), Passive Insulation in Pack	9	2	6	108

Table 5.2: FMEA for High Voltage Battery System

Testing and Demonstration

6.1 FDD.32 Manufacturing and Testing Procedure

6.1.1 Aim and Objectives

6.1.2 Test Description

6.1.3 Testing Infrastructure and Setup

6.1.4 FDD.33 Preliminary Testing Plan

6.2 FDD.20 Demonstration Plan

6.2.1 FDD.22 CAD Renders of Demonstration Setup

6.2.2 FDD.23 Equipment and Infrastructure List

6.2.3 FDD.24 Use of Own Infrastructure